ERDC/CHL TR-00-7

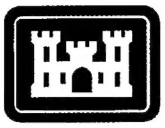

US Army Corps
of Engineers®
Engineer Research and
Development Center

Unrestrained Cylinders Rolling in Steady Uniform Flows

Jack E. Davis

April 2000

Coastal and Hydraulics Laboratory

ERDC/CHL TR-00-7
April 2000

Unrestrained Cylinders Rolling in Steady Uniform Flows

by Jack E. Davis

Coastal and Hydraulics Laboratory
U.S. Army Engineer Research and Development Center
3909 Halls Ferry Road
Vicksburg, MS 39180-6199

Final report

Prepared for U.S. Army Corps of Engineers
Washington, DC 20314-1000

Engineer Research and Development Center Cataloging-in-Publication Data

Davis, Jack E.

Unrestrained cylinders rolling in steady uniform flows / by Jack E. Davis ; prepared for U.S. Army Corps of Engineers.

134 p. : ill. ; 28 cm. — (ERDC/CHL ; TR-00-7)

Includes bibliographic references.

1. Cylinders — Hydrodynamics. 2. Hydrodynamics — Mathematical models. 3. Hazardous waste site remediation. I. United States. Army. Corps of Engineers. II. Engineer Research and Development Center (U.S.) III. Coastal and Hydraulics Laboratory (U.S.) IV. Title. V. Series: ERDC/CHL TR ; 00-7.

TA7 E8 no.ERDC/CHL TR-00-7

PREFACE

This report discusses the dissertation research work performed during the period 1995 to 1999 by Jack E. Davis (U.S. Army Engineer Waterways Experiment Station (WES)), in cooperation with Scott A. Fenical (Pacific International Engineering, Inc., Edmonds, WA), and Drs. Billy L. Edge and Jun Zhang (Texas A&M University, College Station, TX). The work was requested and sponsored by the WES Laboratory Discretionary Research Program . The WES has now become part of the U.S. Army Engineer Research and Development Center (ERDC).

This report is a dissertation in partial fulfillment of the requirements for the degree of Doctor of Philosophy in Ocean Engineering from the Office of Graduate Studies of Texas A&M University. Dr. Edge chaired the advisory committee guiding the research reported herein. Other members of the committee providing technical guidance included Drs. Martin C. Miller, Robert E. Randall, and Jun Zhang. In addition, Dr. H. C. Chen of the Ocean Engineering Program staff contributed scholarly advice particularly in the numerical parts of the research. Dr. Arik B. Engin of DANTEC Measurement Technology, Inc., Mahwah, NJ, provided assistance in setting up and running the particle-image velocimetry laboratory studies. The research was conducted under the general supervision of Ms. Joan Pope, Chief of the Coastal Evaluation and Design Branch, Mr. Thomas Richardson, Deputy Director & Chief of Staff for the Coastal & Hydraulics Laboratory (CHL), and Dr. James R. Houston, Director of the CHL.

At the time of publication of this report, Dr. Lewis E. Link was Acting Director of ERDC, and COL Robin R. Cababa, EN, was Commander.

TABLE OF CONTENTS

LIST OF FIGURES

FIGURE Page

FIGURE Page

LIST OF TABLES

CHAPTER I

INTRODUCTION*

In this report, the motion of smooth, unrestrained circular cylinders, on a smooth, horizontal bed in uniform, steady flow is investigated. The cylinders have specific weights significantly greater than water so that they remain on the bed. The characteristics of general interest in this problem include the forces that act on such cylinders and the characteristics of the nearby flow field, the cylinder's terminal velocity, and the type of motion (e.g., rotation, translation, saltation, or a combination). These characteristics are investigated experimentally and numerically.

This research topic was developed as a result of concerns over the detection, treatment, and removal of unexploded ordnance in aquatic environments. Ordnance remediation projects have shown that a better understanding of the motion of cylinders (the approximate shape of ordnance) in flows would benefit remediation. For example, if the motion of cylinders could be predicted, the region of ordnance mobility could be specified and transport rates estimated. Based on mobility and transport-rate estimates,

---

This dissertation follows the style and format of the ASCE *Journal of Hydraulic Engineering*.

*Parts of this chapter are reprinted with permission from "Terminal velocity of cylinders rolling in uniform flows" by Davis, J. E., Fenical, S. A., Zhang, J., and Edge, B. L., published in the *J. of Hydraulic Engineering*, September 1999, 125(9), 943-952.

sites requiring remediation could be prioritized and the design of engineering works to trap ordnance could be improved (Pope, 1996).

Besides lacking a basic understanding of the characteristics of cylinders moved by a current, predicting the movement of cylinders in natural environments is made more complex by a lack of understanding of the influence of the bottom materials and topography (e.g., clay bed, rippled sand, or bedrock). In thorough research reviews, virtually no pertinent information could be found on the motion of cylinders in flows. Therefore, to begin building the basic principles for flow-induced motion of unrestrained cylinders, the present study simplifies the real-world problem. It offers a first step in understanding the motion of unrestrained circular cylinders in steady flows.

This study has three significant parts. The first part of the study focuses on the laboratory measurement of the motion of cylinders and the characteristics of the flow around moving cylinders. The next part of the study develops an estimate for the terminal velocity of cylinders based on inviscid-flow theory. Although rather restrictive assumptions are made to apply inviscid-flow theory, the result is consistent with the experimental data. The last part of the study is a numerical simulation of the flow field around rolling cylinders and the forces that act on them under certain conditions. Each part of the study provides unique insights into the phenomena associated with the unrestrained motion of a cylinder.

Two types of experiments were conducted. The first experimental study was primarily directed at the measurement of the terminal (maximum) velocity that a given cylinder will achieve in a specified flow. In these experiments, video was used to record the motion of cylinders as they rolled along the horizontal bed of a flume under the force of a steady uniform flow. The video images were processed to determine the speed of the cylinder in each test and the characteristics of the cylinder's motion. The experiments showed that for all of the cylinders, a free-stream velocity threshold (defined as the critical threshold velocity) had to be exceeded for incipient motion of the cylinder. Above a higher free-stream velocity (defined as the super threshold velocity), the cylinder velocity and free-stream velocity approached a constant ratio. Between the critical and super thresholds, the ratio was a function of the free-stream velocity, and the density and diameter of the cylinder. The tests also showed that the cylinders remain in contact with the bed once rolling is initiated. An interesting phenomena referred to as back-sliding was recorded. Essentially, the cylinder rotated at a higher rate than implied by its translational velocity. Some observations of cylinder acceleration were also made which suggest that cylinders will respond quickly to the fluid forces.

The video-image processing was not capable of measuring the flow characteristics around the cylinder as it rolled. Therefore, a second experimental study was directed at the measurement of the flow field. Experiments were conducted similar to the video experiments, but particle-image velocimetry (PIV) was used to measure the

flow field. In the PIV experiments, a laser-camera system was used to measure a two-dimensional plane in the flow. Lasers illuminated seed material (particles) in the flow and a digital camera recorded sequential images of the particles milliseconds apart. The change in position of particles from one image to the next at discrete points in the flow plane provided the instantaneous flow velocities at those points.

The PIV measurement system was at a fixed location in the flume, so a series of flow-velocity measurements were taken as the cylinder approached, passed through, and continued past the field of view of the camera. Hence, the flow fields downstream, around, and upstream of the cylinder were measured, respectively. Additionally, the speed of the cylinder could be determined if specific points on the surface of the cylinder could be seen in more than one set of photographic images. This added to the dataset developed during the video experiments.

Reviews of previous research suggested that the moving surface of the cylinder as it rolled would suppress flow separation. Therefore, it was assumed that under these conditions the boundary layer flow next to the cylinder surface was confined to a thin layer and so inviscid flow theory might be applicable to describe the flow around the cylinder. The results from the PIV measurement of the flow verified that separation was indeed eliminated and the flow had characteristics like those of an inviscid-flow.

Inviscid-flow theory was used to describe the speed of the fluid around the cylinder. The terminal velocity of the cylinder was determined analytically by finding the cylinder rotation that made the speed of the cylinder surface everywhere at least as fast as the speed of the fluid adjacent to it. It was assumed that under this condition, separation could not occur and the drag force would be minimized. Without drag accelerating the cylinder, the terminal velocity would be attained. Inviscid flow theory suggests that this will occur when the cylinder is rolling at 71% of the free-stream velocity. The experiment data was scattered between 60% and 80%.

Neither the experiment measurements nor inviscid-flow theory were able to yield the magnitude of the forces acting on the cylinders. In the experiments, no practical means of instrumenting the cylinders to measure the forces was found. Any instrument mounted on or within the cylinder would have affected the motion of the cylinder, and by the nature of inviscid-flow theory it can not produce a horizontal force in this problem. Therefore, another means of investigating the forces acting on the cylinders was necessary. Numerical simulations were used. The simulations were simple representations of the problem and were aimed at determining the forces on the cylinders when they achieved the terminal velocities recorded in the laboratory experiments. The simulations were used to verify that at the terminal velocities measured in the experiments the moment about the contact point between the cylinder and the wall was near zero and the downstream directed forces on the cylinders were small.

A review of existing research is provided in the next chapter prior to the presentation of the laboratory experiments, inviscid-flow theory, and numerical simulations. While virtually no literature is available regarding the unrestrained motion of cylinders in a flow, some of the concepts and observations of previous fluid mechanic studies of fixed cylinders in flows are useful and are presented.

CHAPTER II

BACKGROUND*

The circular cylinder's symmetrical form and simple mathematical description has made it a desirable shape to study throughout the history of fluid mechanics. It serves as the basis for many mathematical transformations (Milne-Thomson, 1968). Its large moment of inertia, when used in structures, has made it a desirable structural cross-section where loads might be applied from any direction (e.g., smoke stacks, water towers, bridge and pier pilings, offshore structures, and pipelines). Consequently, the literature is filled with studies of the flow forces that act on cylinders and the influence of different fluids and flow regimes on those forces. The literature is replete with information on cylinders restrained from motion, limited to small motions (e.g., transverse or rotary oscillations of cylinders in a flow), or having prescribed motions, where the motion is due to external forces besides that of the flow. Surprisingly, though, no directly applicable literature was found regarding the motion of unrestrained cylinders in flows.

The only studies that gave consideration to unrestrained cylinders were Havelock (1949) where inviscid-flow theory was applied to determine the orbital motion of a

*Parts of this chapter are reprinted with permission from "Terminal velocity of cylinders rolling in uniform flows" by Davis, J. E., Fenical, S. A., Zhang, J., and Edge, B. L., published in the *J. of Hydraulic Engineering*, September 1999, 125(9), 943-952. Copyright 1999 by the American Society of Civil Engineers (see Appendix II).

neutrally-buoyant cylinder beneath free-surface waves, and Tezduyar et al. (1992a & 1992b) where the numerical solution for a two-dimensional cylinder drifting in a very low-Reynolds number flow is presented. An interesting investigation of the movement of round (almost spherical) rocks in stream flows was found (Fahnestock and Haushild, 1962). Though it lacked details and had limited application to the present problem, it may provide useful information for future investigations of cylinder motion on a sand bed. Though directly applicable literature is not available, it is helpful to review the mechanics of flows around and the forces on restrained cylinders as outlined in the literature to gain insight into what might be expected for unrestrained cylinders.

The characteristics of the flow field around restrained cylinders in unbounded steady and unsteady flows have been well studied (see Sarpkaya & Isaacson 1981). Studies can also be found that investigate flows around cylinders in the vicinity of a wall (e.g, Brown 1967, Grace 1971, Yamamoto and Nath 1973, Yamamoto et al. 1974, Sarpkaya and Rajabi 1979, Knoll and Herbich 1980, Fredsøe and Hansen 1987, Taniguchi and Miyakoshi 1990, Sumer et al. 1991). The investigations consider steady and unsteady flow forces acting on restrained cylinders frequently with a small gap between the cylinder and the wall. Davis & Ciani (1976) provide a good review of the literature through the date of their publication. A few studies consider the influence of rotation of the cylinder on the forces (with and without coincident oscillation) and on the flow fields around those cylinders, but none of the studies consider the added influence

of a wall (e.g., Goldstein 1965, Milne-Thomson 1968, Badr et al. 1990, and Tokumaru and Dimotakis 1993).

When a cylinder is restrained in an unbounded steady flow with sufficiently high Reynolds number, the wake of the cylinder formed by separation of the boundary layer will contain vortices of roughly equal strength alternately shed from the top and bottom of the cylinder. When the cylinder is brought within two diameters of a wall, the cylinder's wake is affected (Grace 1971 and Bearman and Zdravkovich 1978). Yamamoto et al (1973) showed that the strength of the vortex shed nearest the wall decreases in strength as the cylinder approaches the wall. Sumer et al (1991), Bearman and Zdravkovich (1978), and Fredsøe and Hansen (1987) state that when the gap between the cylinder and the wall is less than 0.3 diameters, vortex shedding is suppressed. When the cylinder is in contact with the wall, the flow becomes steady and the influence of the wake extends about six diameters downstream (Fredsøe and Hansen 1987). As the cylinder approaches the wall, the stagnation point moves from the middle of the cylinder toward the wall. When the cylinder actually touches the wall a small separation bubble forms on the upstream side of the cylinder limiting the migration of the stagnation point toward the wall (Fredsøe and Hansen 1987). Bearman & Zdravkovich (1978) note that prior to contact with the wall the lower separation point on the cylinder moves toward the downstream side of the cylinder and the top separation point moves about the same distance upstream. This seems to be supported by Hafen (1975) where the upper

separation point was about 70° above the middle of the cylinder. The upper separation point for a wall-free cylinder occurs at about 80° for a laminar boundary layer (Schlichting 1968).

As a cylinder is brought near a wall the lift force on the cylinder is increased. Yamamoto et al (1973) (see also Müeller 1929) showed by inviscid-flow theory that the lift force will be negative (toward the wall) and increase toward negative infinity as the cylinder is brought infinitely close to the wall due to the increasing velocity (and decreasing pressure) beneath the cylinder. As soon as the cylinder touches the wall, inviscid flow theory predicts a positive and finite lift force. Yamamoto et al. (1973) state that in real flows the transition in lift is probably smoother by pointing to the work of Cornish and Jex (1968) which suggests that the lift force might become slightly negative, but as the gap is reduced the force will become positive even before the gap is entirely closed. Arie and Kiya (1967) showed that a shear flow (which is expected near a wall) could cause the lift force to be always positive. Fredsøe and Hansen (1987) note from experimental measurements that the velocity of the flow beneath a cylinder near a wall is approximately the same as the velocity over the top of the cylinder. Hence, there is no difference in pressure distribution on the top and bottom of the cylinder, therefore no net contribution to the lift (positive or negative) is generated. They argued that the positive lift force is due to the stagnation point migrating toward the lower portion of cylinder.

In addition to the influence of the bed, the effect of the moving surface of the cylinder has to be considered. Early researchers conducted experiments with cylinders in an attempt to demonstrate techniques for controlling separation of the boundary layer (Prandtl and Tietjens 1957, Schlichting 1968, and Goldstein 1965). One experiment is particularly pertinent. W.S. Farren (see Goldstein 1965) conducted an experiment with a circular cylinder positioned at the corner of a block as shown in Fig. 1. When the cylinder was rotated, separation was eliminated around the corner of the block. In more recent studies, Modi et al. (1990, 1991b) showed how rotating cylinders at certain points along an airfoil controlled separation and resulted in increased lift and stall angles for the foil. Modi et al. (1991a) investigated the flow past bluff bodies. They showed that the drag on a flat plate perpendicular to the flow could be reduced as much as 75% when rotating cylinders were placed on the upper and lower edges of the plate. The experiments were conducted in a wind tunnel at Reynolds numbers of 30,000 and flow visualization clearly showed the near elimination of a downstream wake. Similar work was conducted by Munshi et al. (1996).

Based on the above reviews it is expected that when an unrestrained cylinder on a wall reaches a certain speed the movement of its surface will suppress flow separation. When flow separation is eliminated, the drag force will be drastically reduced such that the net forces on the cylinder are zero and its terminal velocity will have been achieved. With regard to lift forces, the rotation of the cylinder might increase the lift. However, as

the speed of the cylinder increases, the relative speed of the free-stream flow decreases which would tend to reduce lift for a cylinder adjacent to a wall. To explore the motion of cylinders in a flow, laboratory experiments were designed to measure the acceleration and terminal velocity of cylinders in a flow, the characteristics of their motion, and the flow field around them. The experiments are discussed in the next chapter..

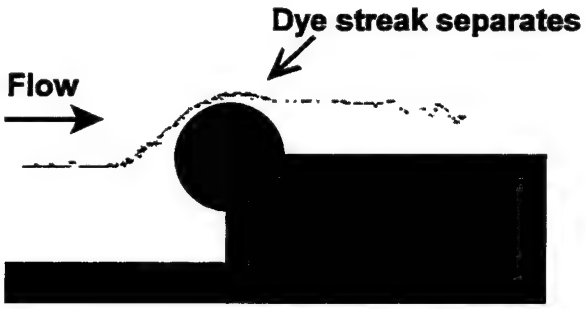

(a) No cylinder rotation

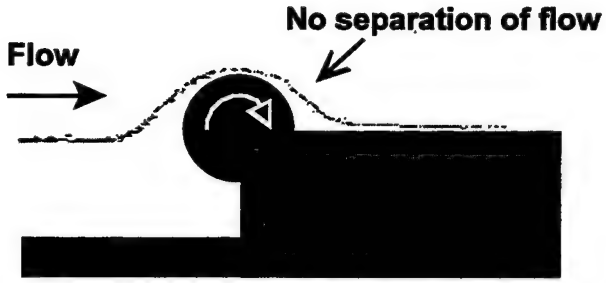

(b) Cylinder rotation

FIG. 1. W. S. Farren's result. Separation is eliminated when the surface of the cylinder is moved with the flow (after Goldstein 1965).

CHAPTER III

EXPERIMENTS*

Introduction

Two different experiments were conducted in a laboratory flume. In the first experiment, video was used to record the motion of unrestrained cylinders under the force of steady, uniform flows. The video images were processed to measure the incipient motion threshold velocity for the cylinders, and their maximum velocity and acceleration. Fenical (1996) provides a good description of the video experiments. In the second experiment, a particle-image velocimetry (PIV) system was used to measure the speed of the cylinders and the flow fields around them as they rolled along the flume. A general description of the laboratory facilities is provided below followed by descriptions of the two experiments and the results.

Experimental Set Up

The laboratory experiments on unrestrained cylinder motion were conducted in a flume at the Texas A&M University Hydromechanics Laboratory. The flume was 36.6 m long, 0.47 m wide and 1.22 m deep. The center of the flume had a 0.15 m-high false bottom with a 1V:12H transition section far enough upstream to allow the velocity

*Parts of this chapter are reprinted with permission from "Terminal velocity of cylinders rolling in uniform flows" by Davis, J. E., Fenical, S. A., Zhang, J., and Edge, B. L., published in the *J. of Hydraulic Engineering*, September 1999, 125(9), 943-952. Copyright 1999 by the American Society of Civil Engineers (see Appendix II).

profile to fully adjust to the changing bottom elevation prior to reaching the experimental section near the center of the flume. The false bottom was covered with a sheet of 6.4 mm Plexiglas™ which provided a smooth, horizontal surface. A 0.87-m wide glass viewing window was provided in the side wall of the flume where the measurements were made. The flume is schematically depicted in Fig. 2.

The water temperature throughout the experiments was constant at 31.7° C. The depth of flow in the flume was maintained at 0.52 m for all of the experiments by a downstream flap gate. The flowrate was controlled by a 1770 rpm centrifugal pump which discharged into the upstream end of the flume at a maximum rate of 0.31 m^3/sec. Velocities were measured using an Acoustic Doppler Velocimeter (ADV) system mounted on a carriage above the flume. The ADV sampled at 25 Hz and provided a velocity value for a given point in the flow. Vertical velocity profiles were measured in the flume with the ADV to observe the characteristics of the profile, particularly the near-bed logarithmic portion of the profile and the relatively constant portion of the profile higher in the flow. Figure 3 provides examples of the profiles measured by the ADV. During the video experiments only a single velocity value was recorded by the ADV at a height 0.30 m above the bed of the flume. This is referred to as the free-stream velocity. The ADV was used in the PIV experiments to roughly set the flow velocity in an experiment. The PIV instruments were used to measure the final velocities as described later.

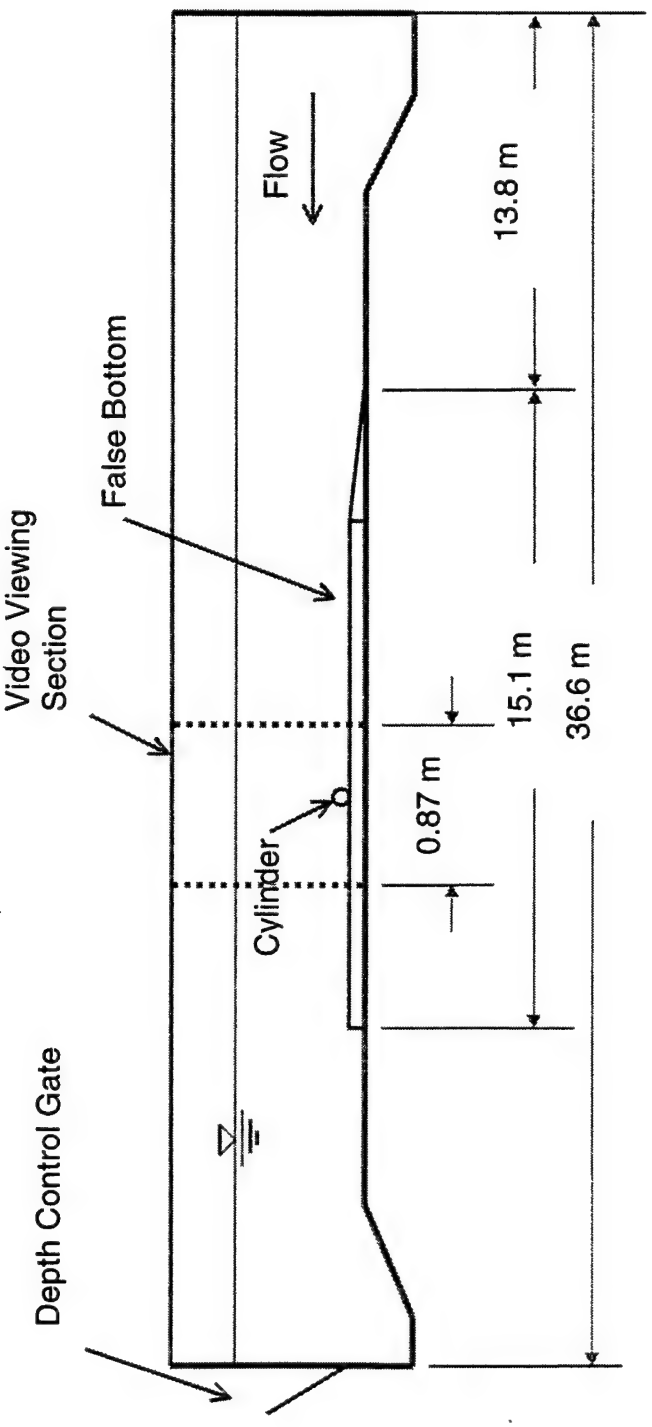

FIG 2. Layout of experiment flume (not to scale).

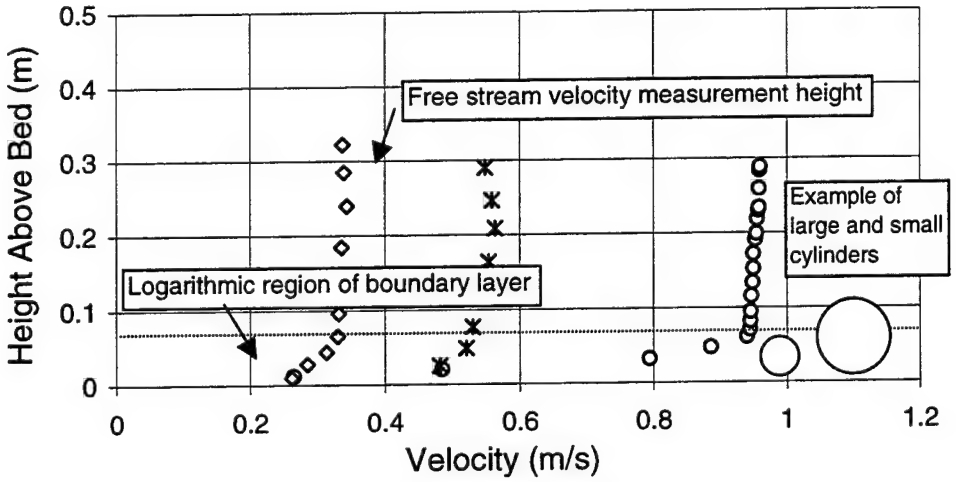

FIG. 3. Velocity profiles measured with the ADV during the video experiments.

In each test, a single cylinder was released from rest in the flow upstream from the viewing window. The cylinder rolled with the flow and passed through the viewing area. The characteristics of the cylinder motion were recorded during the video experiments and the flow-field around the cylinder was recorded in the PIV experiments. For the terminal velocity measurements, a release point was found upstream from the viewing area such that the cylinder reached its terminal velocity prior to entering the viewing area. A sufficient release point was found during preliminary tests by checking for constant cylinder velocities in the viewing area for given upstream release locations. For the cylinder acceleration measurements made during the video experiments, the cylinders were released at the upstream end of the camera's view.

In the tests, several cylinder diameters and specific gravities were used. All cylinders were smooth and all were of the same length. The characteristics of the eight cylinders used in the tests are provided in Table 1. Although the specific gravity for each cylinder was different, they roughly fell into two groups. Four cylinders were made of sand-filled PVC pipe and the other four were made of sand-filled steel pipe. The ends of the pipes were covered with flat 2.55-mm thick acrylic caps that were flush with the surface of the pipes. The sand used to fill the cylinders was sorted with a U.S. Standard Testing Sieve ASTM E-11 set between the #80 and #40 sieve to ensure that the density distribution inside the cylinders was uniform. Due to the width of the flume, all of the cylinders were 0.2 m long. Longer cylinders (up to 0.36 m) were tried, but were rejected because they were affected by the boundary layer of the side walls of the flume. The blockage of the cross-section of the flow by the cylinders was less than 10%.

TABLE 1. Specific gravities of the cylinders used in the experiments.

Diameter(m)	0.048	0.060	0.089	0.115
Steel	3.17	3.01	3.01	2.77
PVC	1.63	1.71	1.57	1.63

Video Experiments

In the video experiments, the displacements, velocities, and accelerations of the cylinders were measured. Fenical (1996) provides a detailed description of the measurements which are summarized here. A Panasonic™ CCD AF Piezo Video

Camera which records directly onto standard VHS tape was positioned to record the cylinders in the viewing section of the flume. The end caps of each cylinder were painted white to increase their visibility in the video images. A set of four black coordinate markers were painted around the perimeter of the end caps at 90° spacing. A fifth coordinate marker was painted in the center. The markers were 6 mm in diameter. A frame of video of a cylinder rolling in the flume during an experiment is shown in Fig. 4.

A Panasonic™ GX4 Multi- Function video cassette recorder (VCR) AG-1950 connected to a Macintosh™ PowerPC 8500 was used to analyze the video images. Selected frames of video were copied to the Macintosh™ PowerPC as image files. The random access memory of the computer (80 MB) was sufficient to store a large number of digitized video images (310 KB each) simultaneously. External storage devices were used to maintain recorded video images.

Once the video images were digitized, the image-processing program NIH Image Version 1.52 (Rasband 1994) was used. The coordinates of the markers on the cylinder end caps were obtained for each video frame analyzed. The markers on the perimeter were used to compute the angular position of the cylinder, while the linear position of the cylinder was obtained by averaging the position of all five markers.

The video and image-processing software were used to determined the position of

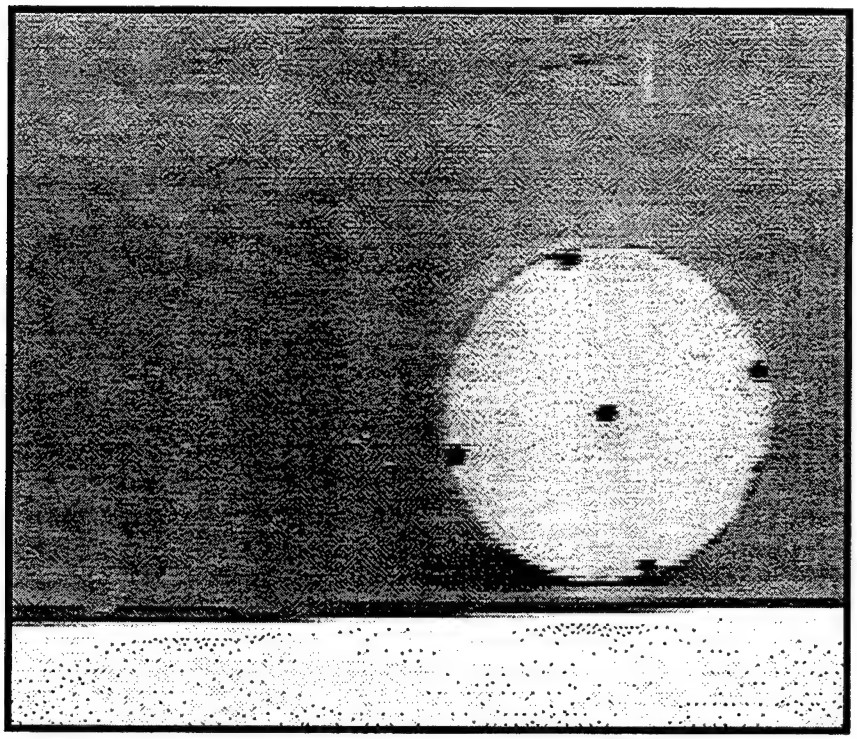

FIG. 4. Black markers on end of cylinder were visible in video experiment.

the coordinate markers on the cylinder end caps from one frame sampled to the next. The velocity was found by finite-difference techniques using displacements and sampling rates. The formulas used are provided below.

$$\overline{X_i} = \frac{1}{5}\sum_{j=1}^{5} X_{ij} \quad , \quad \overline{\theta_i} = \frac{1}{4}\sum_{j=1}^{4} \theta_{ij} \tag{1}$$

$$\overline{V_i} = \frac{\overline{X_{i+1}} - \overline{X_{i-1}}}{2\,\Delta t} \quad , \quad \overline{\omega_i} = \frac{\overline{\theta_{i+1}} - \overline{\theta_{i-1}}}{2\,\Delta t} \tag{2}$$

where the overbar indicates an averaged value, and

X = linear position of cylinder in the direction of flow
θ = angular position of cylinder
Δt = time step (inverse of the sampling rate)
V = linear velocity
ω = angular velocity
i = subscript indicating the time step for which evaluation is being made
j = subscript indicating the marker being evaluated

It is worth noting that when the time step is small, small errors in the position measurement are amplified in the relatively large computed velocity.

Error Assessment

The video-measurement technique had four sources of error which are briefly described here. The errors could be minimized by the selection of proper sampling rates for video frames where the sampling rate is defined as the number of frames analyzed for each second of video recorded. Some errors were minimized by increasing the sampling rate while others were maximized, so optimization of the sampling rate was required.

The first source of error associated with the finite-difference formulas is truncation error due to elimination of higher-order terms in the Taylor series expansions used to derive the formulas. These errors are only significant, though, when accelerations are large as when the cylinders are first released in the flow. The truncation error may decrease with an increase in the sampling rate. The truncation errors inherent in the finite-difference formulas given above were found within the accuracy of the

experimental method.

A second source of error results from the resolution of a pixel. The coordinates of the center of a pixel are recorded as the coordinates for any point selected within that pixel. This error is limited to half the size of a pixel or approximately 0.5 mm. Therefore, if the sampling rate is decreased the percent error relative to the measured displacement is reduced.

A third error is caused by inconsistently selecting the center of the coordinate markers on the ends of the cylinders. In other words, the operator may select a point within the marker but not necessarily the center of the marker. The maximum error was estimated to be 3 mm. Like the pixel-selection error, the relative error resulting from this operator-selection error can be minimized by reducing the sampling rate.

A fourth source of error results from the video equipment used. Riedl (1994) conducted a video-imaging study showing that while standard cameras capture 30 frames-per-second, each frame is not necessarily recorded at 30 Hz. Riedl found that the actual sampling frequency ranged between 29.98 Hz and 30.70 Hz. Therefore, the camera produces a small error in the calculation of cylinder motion because a time-step is used that is based on the assumption that the video frames were recorded at 30 Hz. This error was found to be insignificant and was neglected in this study.

The maximum possible sampling rate was limited by the speed of the camera to 30 frames per second or 30 Hz. While sampling at the maximum rate provides the most detail, it also creates numerically-induced fluctuations in the corresponding velocities discussed above. Several sampling rates were investigated to optimize damping of the fluctuations while providing sufficient data for the analyses. Figure 5 shows the angular velocity (ω) of a cylinder with time. The data presented in Fig. 5 were processed at three different sampling rates. The lower sampling rates removed the fluctuations observed when processing at the highest rate of 30 Hz. To ensure that the fluctuations were indeed numerically-induced and not real fluctuations in the force acting on the cylinder, the motion of a cylinder was analyzed numerically. An analytical equation was fit to the smoothed angular velocity data for one of the cylinders. The analytical equation was then used to generate two artificial displacement datasets. The first dataset contained numbers with accuracy of one micrometer (10^{-6} m), while the second data set had numbers rounded to the nearest increment of 3 mm which was on the order of the largest errors. When the artificial data were sampled at 30 Hz, the low-accuracy data showed the same fluctuations in velocity as the real data set, while the high-accuracy data coincided well with the exact analytical solution. Therefore, it was deduced that the fluctuations found in the data were the result of high sampling rates and measurement errors. Four sampling rates were evaluated in the analysis of data, namely 30, 15, 10, and 5 Hz. It was determined that 10 Hz provided a sufficient number of data to conduct the differencing operations while minimizing the numerically-induced fluctuations.

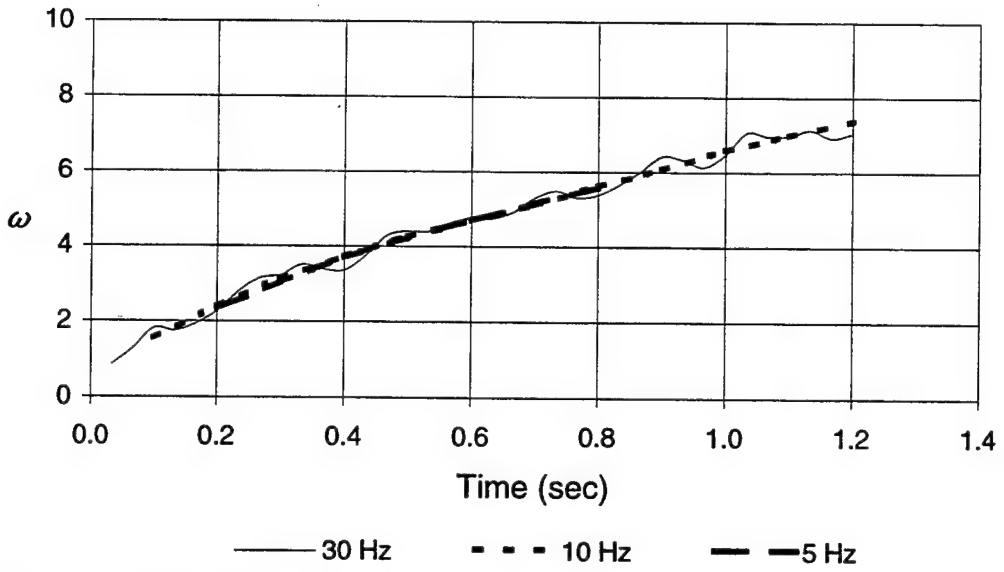

FIG. 5. Artificial oscillation in angular velocity damped by lower sampling rate of video images (after Fenical 1996).

Video-Experiment Results

Terminal Cylinder Velocities

The terminal cylinder velocities and the free-stream velocities (V and U_o, respectively) for all of the experiments are plotted in Fig. 6. The experimental data are provided in Table 2. The figure shows that, even though the bottom of the flume was horizontal and smooth, the free-stream velocity had to exceed a critical threshold value U_c to cause incipient motion of the cylinders. The need to reach a threshold velocity is probably caused by imperfections on the bed such as small, local deformations and unevenness. The critical threshold velocities for each cylinder are provided in Table 2. It is worth noting that the PVC cylinders may have had slightly higher threshold values

than given in the table. As can be seen in Table 2 and in Fig. 6, measurements were made for $U_o = 0.10$ m/s. At that velocity, none of the cylinders moved in the flume. The next free-stream velocity tried was $U_o = 0.14$ m/s under which all of the PVC cylinders rolled. The actual critical threshold for each of the PVC cylinders, may therefore be between 0.10 and 0.14 m/s although they are given in Table 2 as $U_c = 0.10$ m/s.

From the data, it appears that the specific gravity of the cylinders has a significant influence on the magnitude of the threshold velocities. This is consistent with results from sediment-particle transport studies where more dense particles of the same size have a higher threshold velocity (e.g. van Rijn, 1984). The threshold velocity for the steel cylinders was about twice that of the PVC cylinders. Similarly, for a given specific gravity, it would be expected that cylinders with larger diameters would have higher critical threshold velocities. That trend is weakly shown in the data for the steel cylinders, but can not be observed for the PVC cylinders possibly for the reasons of resolution in the threshold velocity previously noted.

TABLE 2. Cylinder parameters and terminal velocities from video measurements (after Fenical 1996).

Number	1	2	3	4	5	6	7	8
Diameter (m)	0.048	0.048	0.06	0.06	0.089	0.089	0.115	0.115
Specific Gravity	3.17	1.63	3.01	1.71	3.01	1.57	2.77	1.63
Critical Velocity (m/s)	0.22	0.10	0.22	0.10	0.24	0.10	0.24	0.10
Flow Velocity (m/s)	Terminal Velocity (*n*)							
0.10	0	0	0	0	0	0	0	0
0.14	0	0.31	0	0.34	0	0.41	0	0.24
0.15	0	0.40	0	0.52	0	0.50	0	0.32
0.17	0	0.48	0	0.45	0	0.45	0	0.35
0.18	0	0.43	0	0.53	0	0.52	0	0.41
0.20	0	0.41	0	0.47	0	0.46	0	0.38
0.22	0	0.54	0	0.54	0	0.54	0	0.51
0.24	0.31	0.5	0.33	0.44	0	0.48	0	0.38
0.28	0.31	0.44	0.27	0.47	0.36	0.57	0.22	0.46
0.31	0.34	0.43	0.34	0.45	0.34	0.50	0.40	0.54
0.34				0.64				
0.35	0.35	0.53	0.37	0.55	0.43	0.63	0.47	0.59
0.36	0.42	0.63	0.51	0.68	0.49	0.64	0.44	0.60
0.37	0.38	0.52	0.36	0.61	0.40	0.67	0.41	0.61
0.49	0.44	0.62	0.49	0.65	0.46	0.69	0.55	0.60
0.52	0.53	0.67	0.59	0.67	0.63	0.71		0.74
0.57	0.50	0.61	0.59	0.70	0.62	0.71	0.57	0.75
0.62	0.63	0.64	0.59	0.74	0.67	0.71	0.66	0.77
0.69	0.59		0.61				0.65	
0.69	0.55	0.61	0.62	0.68	0.61	0.66	0.61	0.70
0.75	0.55	0.62	0.56		0.60		0.61	0.65
0.75	0.53	0.66	0.55	0.65	0.61	0.69	0.61	0.71
0.79	0.63	0.69	0.62	0.70	0.64	0.76	0.71	0.74
0.89	0.60		0.64	0.68	0.65		0.67	0.72
0.89	0.61	0.58	0.61	0.65	0.59	0.77	0.70	0.78
0.89	0.61	0.64	0.62	0.65	0.62	0.79	0.63	0.77
0.92	0.62		0.59		0.66		0.64	
0.98	0.62		0.59		0.67		0.67	
0.98	0.67				0.69		0.68	
1.07	0.70		0.67		0.68		0.71	
1.07			0.66		0.65		0.67	

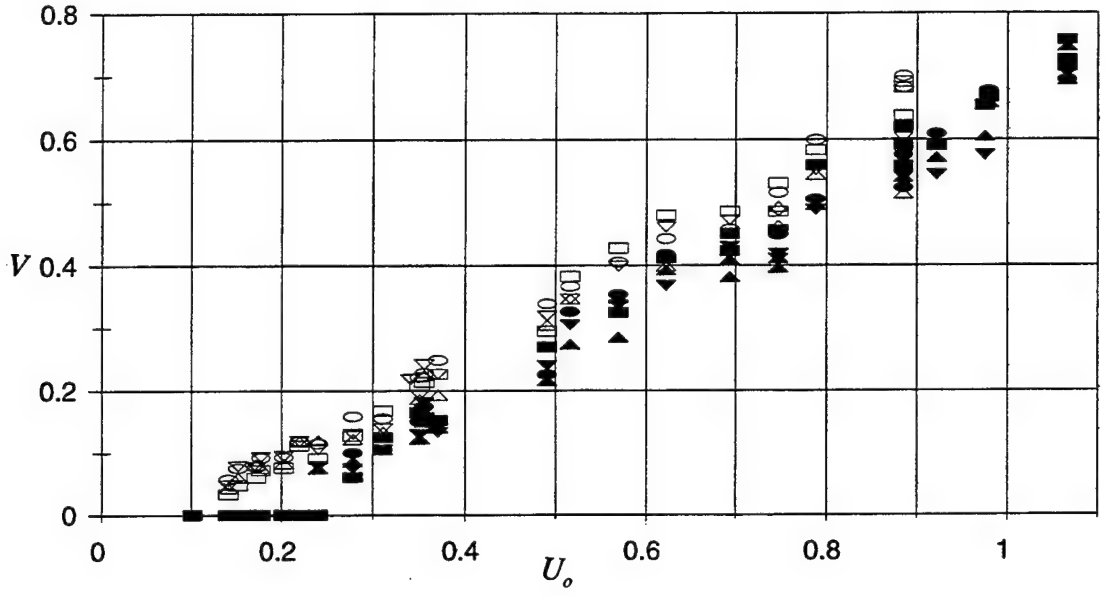

FIG. 6. Relationship between terminal cylinder velocity and free-stream flow velocity (after Fenical 1996).

When the free-stream velocities are greater than the critical threshold in Fig. 6, the data are sorted by specific gravity, as well. The velocities of the steel cylinders are always slightly lower than those for the same-diameter PVC cylinders in a given flow. The data also show trends based on cylinder diameter. For a given specific gravity and at the higher free-stream velocities, larger cylinders tend to have greater velocities than smaller cylinders. This may be because the larger cylinders extend further outside the logarithmic portion of the velocity profile near the bed (Fig. 3). At low flow velocities, smaller cylinders tend to have higher velocities than the larger cylinders. This may be because the forces that resist the motion of the cylinders (submerged weight) still

dominate the cylinder's motion at low free-stream flows. However, the numerical simulations discussed in Chapter V suggest that the flow conditions may also have an influence on the lower velocity ratio at low free-stream flows.

When non-dimensionalized, the data provide additional insights. A convenient non-dimensionalization for the cylinder velocity is the ratio $n = V/U_o$. Several alternatives are possible for non-dimensionalizing the free-stream velocity. The Reynolds number can be used where it is defined as $R = U_o D/\nu$ and where D is the cylinder diameter and ν is the kinematic viscosity of the fluid. The Reynolds number is plotted with the terminal velocity ratio in Fig. 7. Interestingly, the data in the region of higher R approaches a constant n scattered between 0.60 and 0.80. That is, the cylinder speed is between 60% and 80% that of the free-stream flow. At low values of R, the value of n depends on R and the data are more scattered. The Reynolds number does not account for the critical threshold velocity or the specific gravity of the cylinder. Figure 7 shows the segregation of the data by specific gravity.

To account for the critical threshold values, van Rijn (1984) used a mobility parameter that was equivalent to U_c / U_o. For convenience, the inverse of the mobility parameter, U_o / U_c, is used to plot n in Fig. 8. As U_o / U_c approaches unity, the ratio n decreases toward zero. At large values of U_o / U_c, the dependency is diminished and the data asymptotically approach a constant value of n.

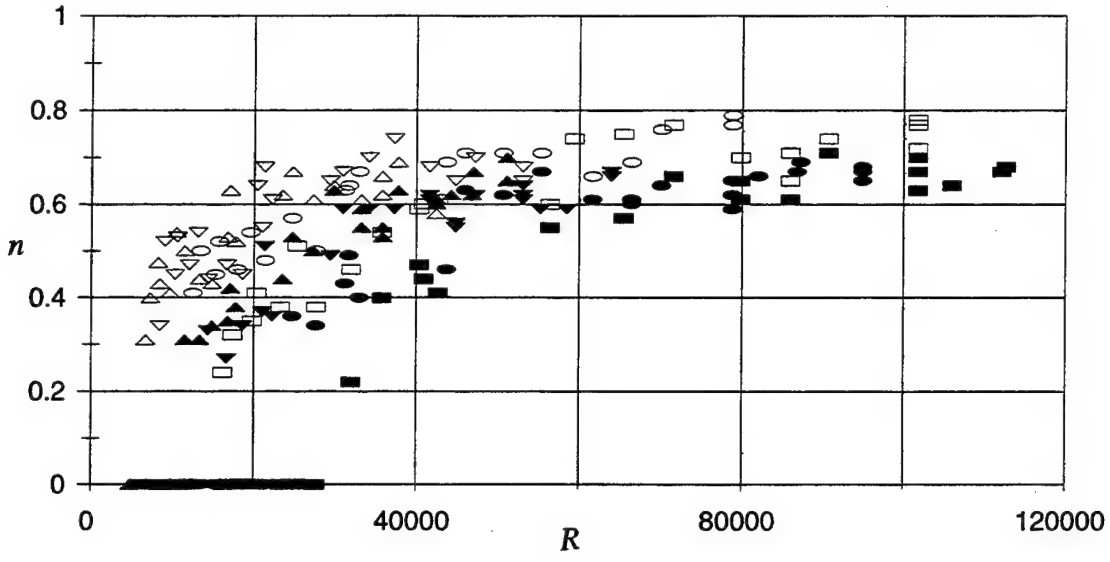

FIG. 7. Cylinder terminal velocity ratio relationship with Reynolds number.

The use of the mobility parameter highlights the tendencies of the data based on the ratio between the free-stream velocity and the velocity required to make the cylinder move but does not explicitly contain the influence of the diameter of the cylinder or its specific gravity. Since the critical threshold velocities for the PVC cylinders were not well determined, another approach using a modified Shields parameter is presented. The

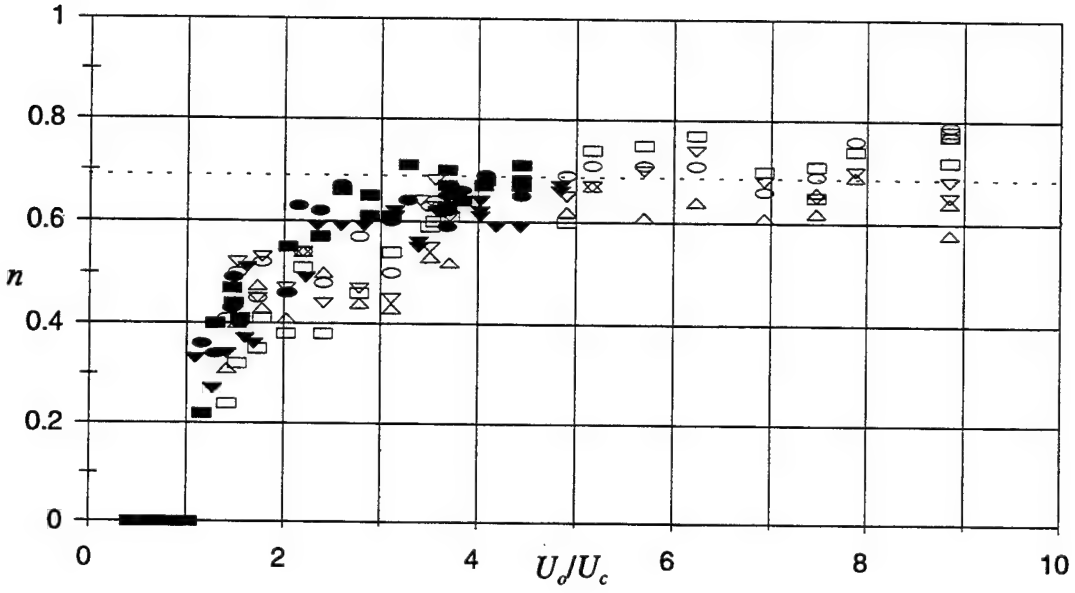

FIG. 8. Cylinder terminal velocity ratio relationship to mobility parameter.

Shields parameter, $\theta = u_*^2 / (S\text{-}1)gD$, provides a useful way to present sediment-transport data (Shields 1936) by relating the destabilizing flow forces to the stabilizing forces. The destabilizing force is represented by the friction velocity u_* which is a function of the bed shear stress. The stabilizing force is the submerged weight of the particle where S and D are respectively the specific gravity and diameter of the particle, and g is the constant of gravitational acceleration. Because the cylinders extend well above the bed and are exposed to forces induced by the higher velocities in the profile, the friction velocity is replaced by the free-stream velocity in the modified Shields parameter, i.e.

$$\theta_o = \frac{U_o^2}{(S-1)\,g\,D} \tag{3}$$

where S and D are now the specific gravity and diameter of the cylinder. van Rijn (1984) actually defined his mobility parameter as $\sqrt{\theta_c/\theta_o}$ where θ_c is the Shields parameter based on the critical threshold velocity U_c^2. Hence, $\sqrt{\theta_c/\theta_o}$ reduces to U_c/U_o. Since the Shields parameter involves the specific gravity and diameter of the cylinders, it should contain the influence of the incipient motion threshold. The same data trends discussed above can be observed in Fig. 9 where the modified Shields parameter is used instead of the mobility parameter.

Influence of Aspect Ratio

The aspect ratio of the cylinders is defined here as the ratio of the length of the cylinders (L) to their diameters (D). In general, non-rotating cylinders with low aspect ratios will have complex three-dimensional wakes (Rooney et al. 1995; Okamoto and Sunabashiri 1992). In contrast, non-rotating cylinders with large aspect ratios have essentially two-dimensional wakes. The narrow flume used in this study required the use of cylinders with small aspect ratios. The aspect ratios for the cylinders used in this study are provided in Table 3. The significance of the small aspect ratio on terminal velocities in these experiments is unknown though some conclusions may be drawn from the PIV data analysis and numerical simulation results discussed later.

TABLE 3. Cylinder aspect ratios and flume blockage ratios.

Diameter (m)	0.048	0.060	0.089	0.115
L/D	4.23	3.39	2.28	1.77
% Blockage	4.0	5.0	7.4	9.6

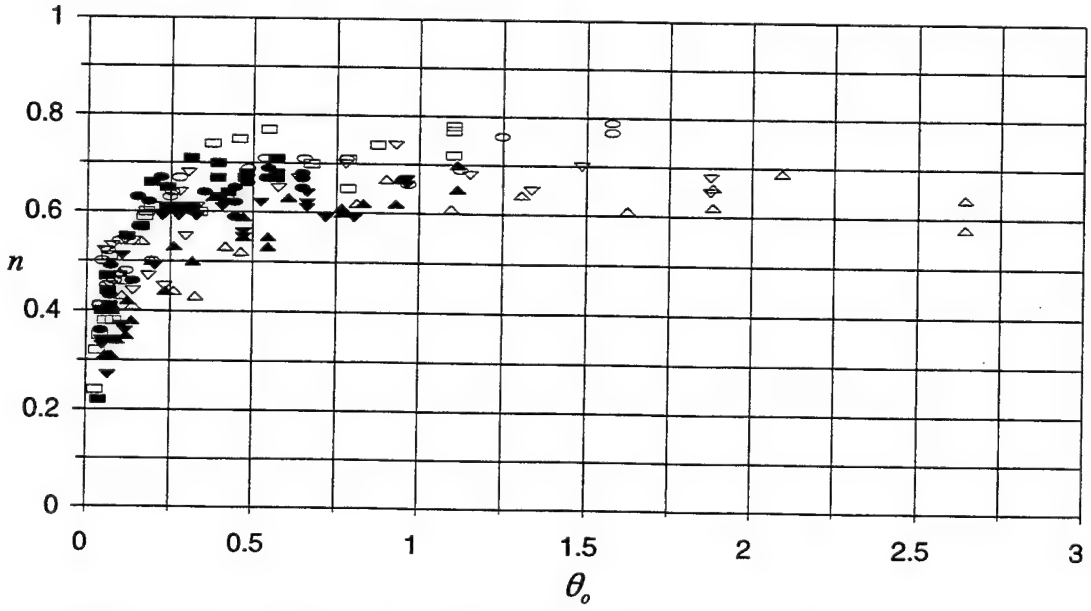

FIG. 9. Cylinder terminal velocity ratio relationship to modified Shields parameter.

Influence of Blockage Ratio

Previous studies such as Skotner et al. (1994) have indicated that the forces

exerted on cylinders in currents increase as the blockage ratio increases. The blockage ratio is the ratio of the frontal area of the cylinder to the total cross-sectional area of the flow in the flume. Since the depth in the flume remained constant at 0.52 m and the length of the cylinders used were constant at 0.21 m, the blockage ratios of cylinders depended only on the cylinder diameters. Therefore, the influence of the blockage ratio on the terminal cylinder velocities cannot be separated from the influence of diameter on terminal velocity discussed above. However, the blockage ratio was less than 10% even for the largest cylinders as shown in Table 3.

Cylinder Backsliding

Analyses showed that the angular velocities of the cylinders multiplied by their radii was slightly greater than the corresponding average linear velocities, especially for the higher flow velocities. This phenomena was termed backsliding and is shown in Fig. 10 for the 0.115 m steel cylinder rolling at its terminal velocity over a range of free-stream flow velocities. The figure was typical of all eight cylinders tested. The degree of backsliding, or the backsliding velocity, is defined as the difference between the average translational velocity and the average angular velocity multiplied by the radius. Figure 10 shows that the backsliding velocity increased with increasing terminal velocity.

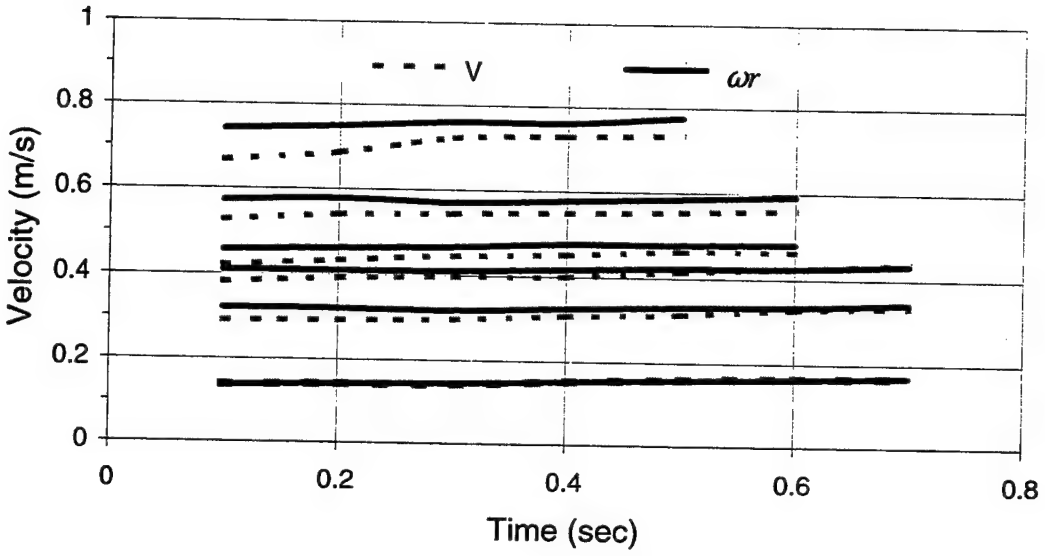

FIG. 10. The backsliding velocity increased with increasing terminal velocity (after Fenical 1996).

Cylinder Acceleration

During the experiments a few tests were conducted to measure the acceleration of the cylinders from rest. In the tests, the cylinders were released at the upstream end of the viewing section of the flume and recorded by video. The acceleration was calculated like the velocity, using a finite-difference form of the second derivative of displacement. The results were unsatisfactory in that artificial oscillations in the acceleration were quite large. An example of the acceleration for a cylinder is plotted in Fig. 11. The oscillations in acceleration were caused by the same factors that caused oscillation in the

velocity (first derivative of displacement) which were discussed in the previous section on video-image measurement errors. The oscillations could be minimized by a lower sampling rate of the video images, but would result in insufficient data for complete analysis.

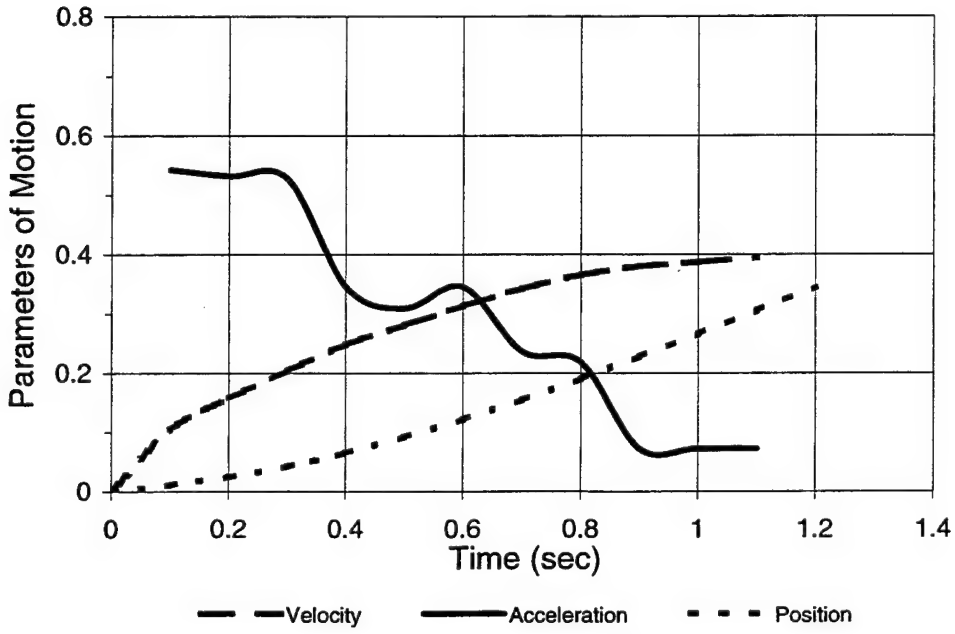

FIG. 11. Displacement, velocity and acceleration for a cylinder (after Fenical 1996).

Even if a good calculation of the acceleration had been possible, it would still have been difficult to interpret the results. During the tests, prior to release, the cylinders were held in place by a screen. While the screen prevented downstream movement of the cylinder, it did not prevent their vertical movement which under high flows was

considerable. The cylinders often bounced up and down prior to release. Therefore, it was difficult to ensure that all cylinders started in the same position. Also, as the screen was moved out of the way, it had an unknown influence on local flow which may have influenced the acceleration of the cylinders. For these reasons, the study of cylinder acceleration was not pursued. However, Fenical (1996) reports some of the measurement results.

The tests did provide an interesting and possibly useful insight, however. From Fig. 11, it is clear that the cylinder accelerated quickly. The figure shows that the cylinder reached its terminal velocity in approximately one second after release. This was observed in all of the experiments for both steel and PVC. The implication is that a cylinder responds quickly to flow conditions. For example, under oscillatory flows, where a peak flow velocity is reasonably maintained for a few seconds, a cylinder may have sufficient time to reach its maximum velocity.

PIV Experiments

The PIV System and Operation

The PIV experiments used the same range of flow conditions and cylinders as the video experiments described previously with the exception that the 0.048 m and 0.089 m steel cylinders were damaged between experiments and could not be used in the PIV experiments. Each experiment proceeded by setting the flow velocity in the flume as

measured by the ADV. As in the video experiments, the cylinders were released upstream from the measurement area and allowed to roll freely with the flow toward the measurement area. As the cylinders passed through the viewing area, measurements were made with the PIV system. One test was conducted to measure the flow field in the wake of a stationary, non-rotating cylinder.

The PIV measurement system used for these experiments was developed by Dantec, Inc. The experimental setup is depicted in Fig. 12. Two pulsed Nd:Yag lasers that project a plane of light (as opposed to a narrow beam of light) were mounted over the flume on a secure brace. The plane of laser light was centered in the flume, parallel to the axis of the flume, and in front of the viewing window. The lasers shown down into the water through a glass-bottomed box. The box skimmed the surface of the water in the flume creating a clear, undistorted view into the water. The box was positioned such that it created minimal surface disturbances.

A cross-correlation digital camera was mounted in front of the viewing windows in the side of the flume. Its view was perpendicular to the plane of the laser light. The lasers and camera were synchronized by the Dantec PIV 2000 Processor which was connected to a personal computer. The computer provided a platform for viewing data as it was acquired and processed, for entering system control commands, and for entering notes for each experiment. The processor had dedicated, highspeed hardware for

processing PIV data, so the data could be collected, processed, and displayed in a near real-time mode. The system used the Dantec Flow Mapping (FlowMap) system-control software to generate images and graphics, as well as the Flow Manager (FlowMan) software for system control, and file and data manipulations.

The field-of-view of the digital cross-correlation camera was approximately 0.1 m by 0.1 m. A scale was established within the images by photographing a ruler illuminated by the laser. The ruler scale was correlated with the image scale given in pixels. The correlation was then used for measuring position with an image. As described in more detail below, the scale was essential for determining the speed of cylinders in the experiments by providing a means of measuring the displacement of the cylinder between sequential images. It should be noted here that the derived scale was only valid along the plane of the laser light.

The two lasers illuminated the flow in bursts just 0.002 seconds apart. The digital cross-correlation camera recorded an image of the flow field with each burst. The image-pair was then passed to the processor where the images were subdivided into interrogation regions. A cross correlation between coincident interrogation regions in each image was made. Particles in the flow within the interrogation regions were identified by the processor as gray-scale values. The change in position of the particles

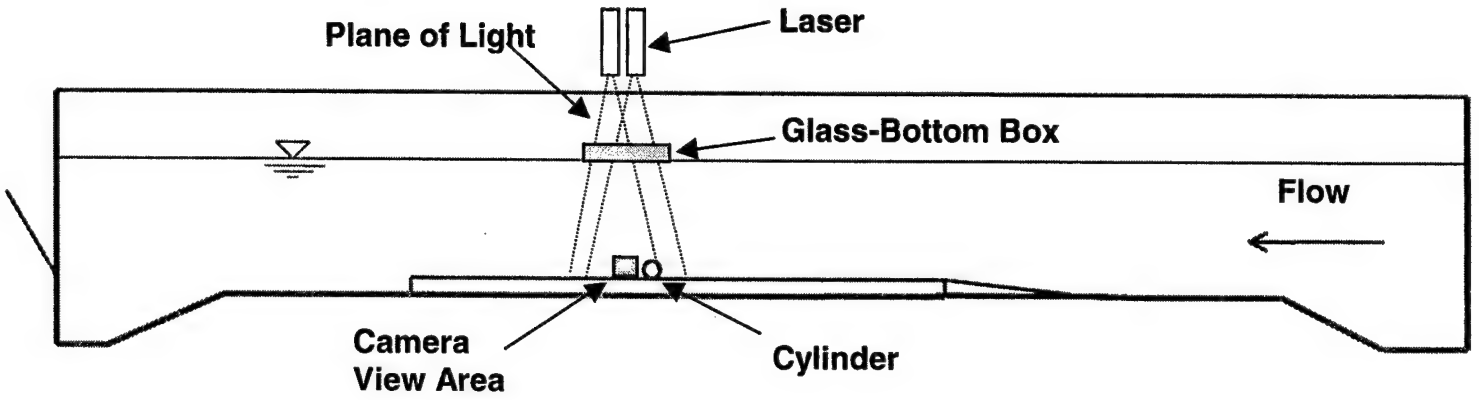

FIG 12. Layout of flume for PIV experiments. Dimensions provided in Fig 2.

from one image to the next was correlated to determine the displacement for that interrogation region. Velocity vectors were derived from the displacements.

A digital image of a rolling cylinder and the computed velocity vectors are shown in Fig. 13. Generally, in cross-correlation PIV analyses, the interrogation regions are in the same locations from one image to the next. However, if the flow velocity is relatively large or the interrogation region relatively small, too many of the particles will leave (or enter) an interrogation region causing poor correlations. To avoid this problem, the interrogation regions defined in the second image were offset downstream by a small distance (when compared to the first image). The offset was based on the nominal flow velocity in the flume times the time interval between images. The technique anticipates the displacement of the particles by shifting the interrogation region in the direction of the flow. In these tests, correlation results were improved by following this procedure.

Since the cross-correlation process relies on evaluating the gray-scales within interrogation regions, errant vectors often occurred very near the cylinder. The cylinder might roll into or out of an interrogation region during the measurement. The data processor could not distinguish the gray of the cylinder's surface from the gray of the particles in the fluid. Sometimes glare from the cylinder surface would obscure the grey-scale of the particles in the nearby flow field. The processor would also evaluate the areas completely filled by the body of the cylinder resulting in vectors that were

obviously not part of the flow. Since all of the errant vectors were very near or coincident with the cylinder, it was easy to identify them and avoid them.

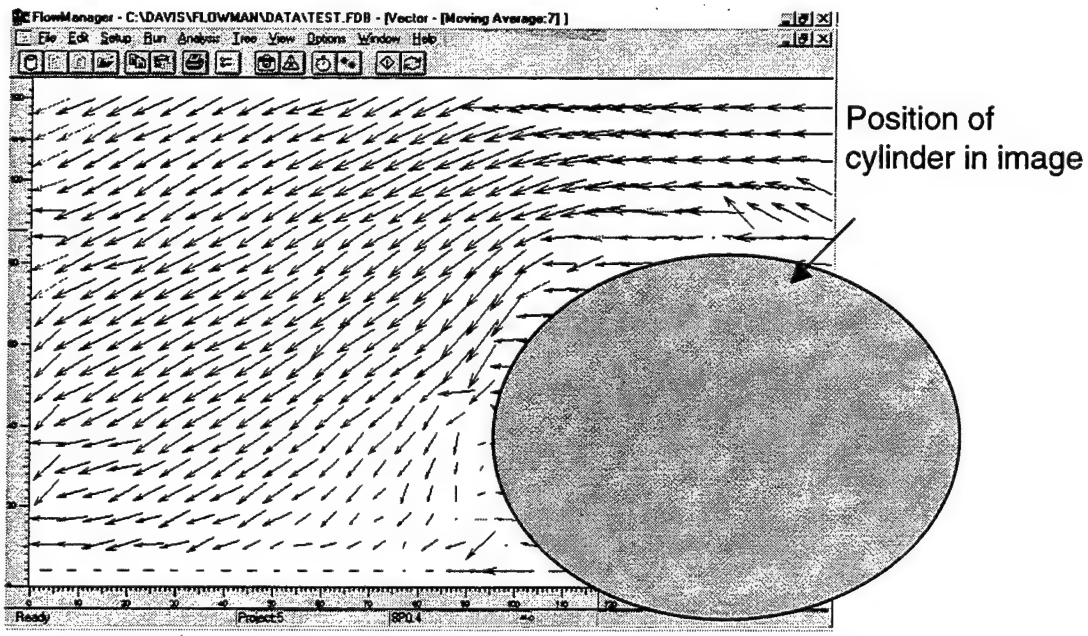

FIG. 13. Vector plot from PIV measurement of flow around cylinder.

During a single experiment, approximately 5Mb of data are acquired and stored. Each digital image-pair is recorded, as well as the computed vector field associated with each corresponding image-pair. The data were stored on the computer hard disk. Each image-pair used 730Kb of hard disk space, while the computed flow fields used another 10Kb. Between 5-10 image-pairs were recorded in each experiment along with their associated velocity-vector plot.

PIV-Experiment Results

Introduction

The PIV data provide information to characterize the flow around the moving cylinder. Several results were obtained from analysis of the PIV data. In particular, the characteristics of the flow over a rolling cylinder, and the terminal velocity ratios of the cylinders were measured. These data were used to enhance the video-experiment data set, and to assess whether the wake of a rolling cylinder could be considered two- or three-dimensional. The techniques used to obtain this information are discussed below.

Filtering Errant Vectors

Errant vectors were sometimes present in the vector field (e.g., Fig. 14). The FlowMap filtering software was used to locate and modify vectors that differed from neighboring vectors. Strong differences indicated an errant measurement. Each vector was compared to all surrounding vectors. An acceptance criteria was used to determine whether the vector under consideration was errant. The criteria in the FlowMap software does not have a physical basis, but is adjusted until the user is satisfied that the software is correcting only obviously errant vectors. If desired, the errant vectors are replaced by vectors derived from an average of the surrounding vectors. Figure 14 shows the results after filtering. Generally, errant vectors occurred very near the cylinder or near the boundary of the image. Only a few errant vectors were found in the center region of the image and away from the cylinder. All velocity vector plots were filtered prior to use in

subsequent analyses.

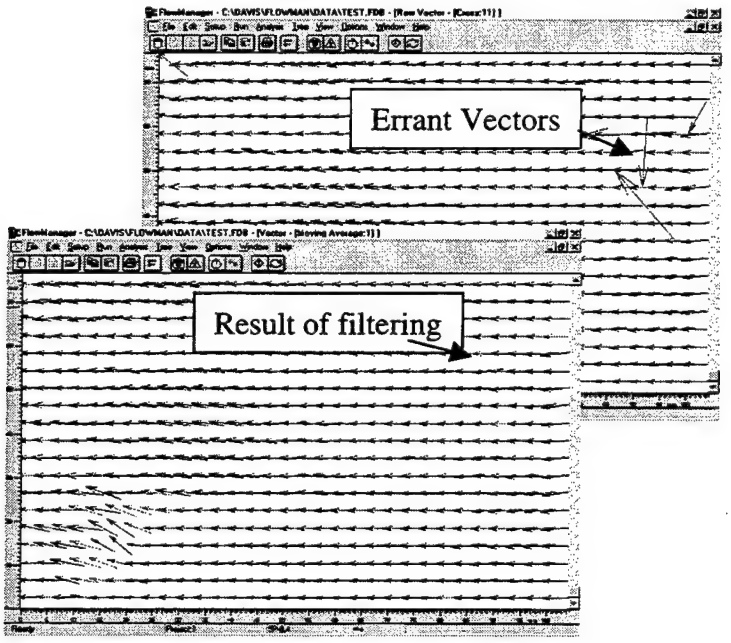

FIG. 14. Errant velocity vectors are modified by averaging the neighboring velocity vectors.

Measurement of the Flow Velocities

Several flow velocity values can be derived from the PIV experiments. One velocity value is the average velocity of the entire vector field derived from the PIV measurement. Another velocity value is the depth-averaged magnitude of a velocity profile extracted from the PIV measurement. (Examples of extracted velocity profiles are shown in Fig. 15 with comparisons to velocity profiles taken during the video experiments.) A third velocity value can be derived from averaging velocities at a given

height in the flow field. In these experiments, a height about 0.064 m above the bed was used. This point was considered outside the logarithmic portion of the boundary layer and in the relatively constant portion of the velocity profile. This was similar to the velocity values recorded by the ADV in the video experiments and was therefore assigned to U_o. The values for U_o measured by the PIV are provided in Table 4 with other data derived from the experiments. To ensure that the measured flow velocity was not influenced by the presence of the cylinder, vector fields were used that were well upstream of the location of the cylinder (i.e., the velocity was measured after the cylinder had passed through the viewing area). In that way, disturbances due to the cylinder are downstream.

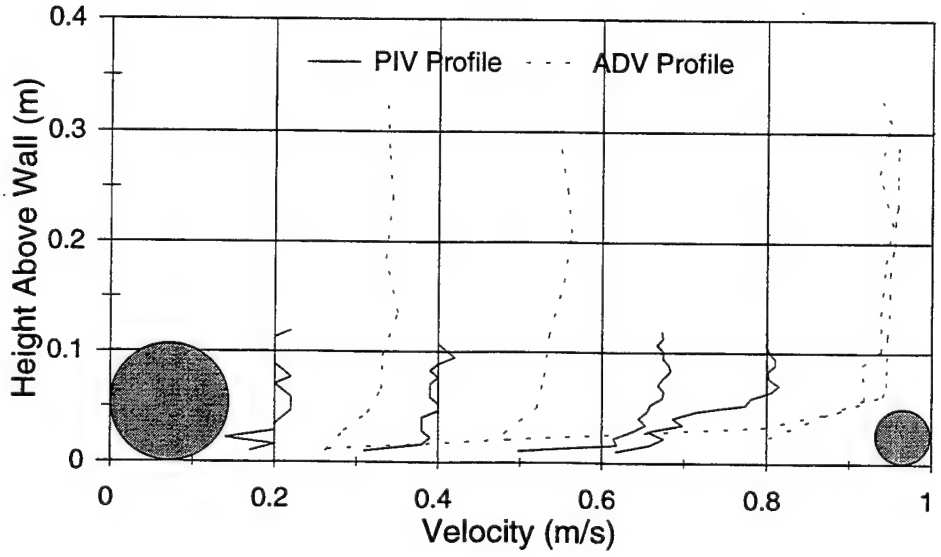

FIG. 15. Velocity profiles from PIV measurements combined with profiles from the video experiments measured with the ADV.

Cylinder Speed

The cylinder terminal velocities were computed using U_o derived from the PIV data. The results are provided in Table 4. Only 15 out of the 46 experiments could be used to determine cylinder speed because the measurement point on the cylinder was often not visible in sequential images. Certain parts of the cylinders had to be visible in consecutive images in order to accurately measure displacement. The change in position of a given point on the cylinder from one image to the next was measured and divided by the time elapsed between the subsequent images which gave the speed of the cylinder. The only point that could be consistently located on the cylinder in sequential images was 90° counterclockwise from the top of the cylinder as shown in Fig. 16. In a few cases, that point was found in the first image, while a point 180° clockwise (one diameter upstream) from that point could be seen in a subsequent image. In these cases, the distance that the first point moved between images was determined by adding the diameter of the cylinder to the position of the second (upstream) point as depicted in Fig. 17.

The terminal velocity of the cylinders are presented non-dimensionally against the Reynolds number (R) and modified Shields parameter (θ_o) in Figs. 18 and 19, respectively, with the video data (from Figs. 7 and 9). The parameters n, θ_o, and R were described in the previous section on video-experiment results. The PIV data are consistent with the results from the video experiments which indicated that terminal

velocity ratios approach a constant value between n = 0.60 - 0.80 for the higher values of R or θ_o, and that n depends on R or θ_o at lower values.

TABLE 4. Cylinder terminal velocity ratios from PIV experiments.

Cylinder	**1**	**2**	**3**	**4**	**5**	**6**	**7**	**8**
Diameter (m)	0.048	0.048	0.06	0.06	0.089	0.089	0.109	0.109
Specific Gravity	3.17	1.63	3.01	1.71	3.01	1.57	2.77	1.63
Critical Velocity (m/s)	0.22	0.10	0.22	0.10	0.24	0.10	0.24	0.10
Flow Velocity (m/s)	**Terminal Velocity Ratio**							
0.64		0.72						
0.43			0.63					
0.83			0.71					
0.56			0.37					
0.43			0.63					
0.43				0.72				
0.26				0.65				
0.26				0.65				
0.26				0.54				
0.68						0.74		
0.68						0.75		
0.42						0.74	0.64	
0.22						0.68		
0.80							0.71	
0.68								0.74

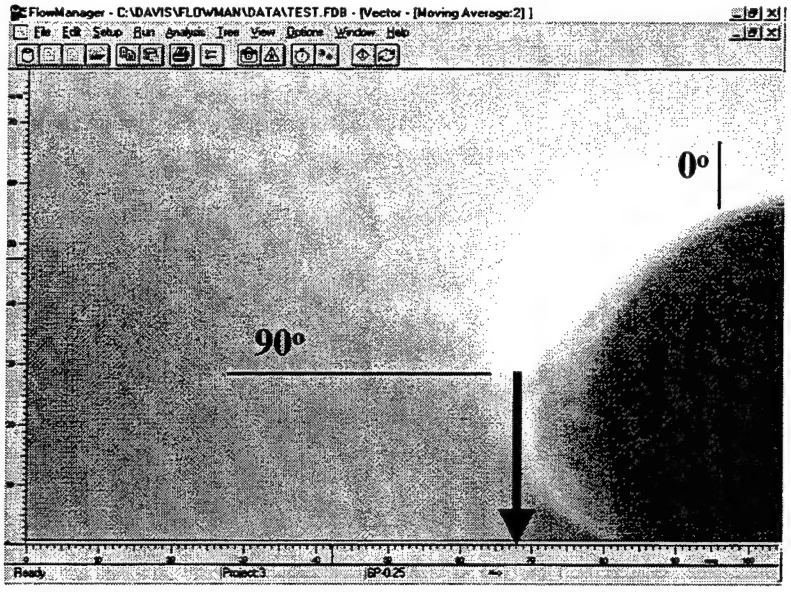

a)

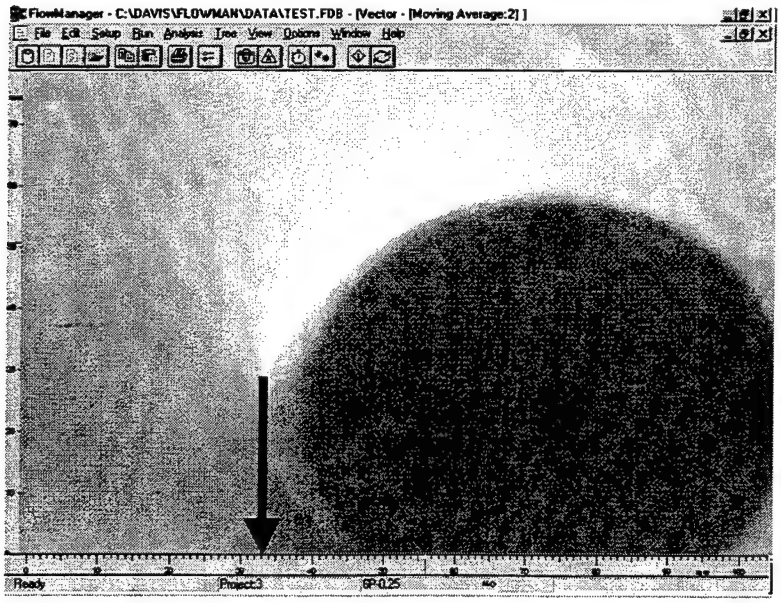

b)

FIG. 16. Displacement of cylinder found by measuring change of position of cylinder in sequential images.

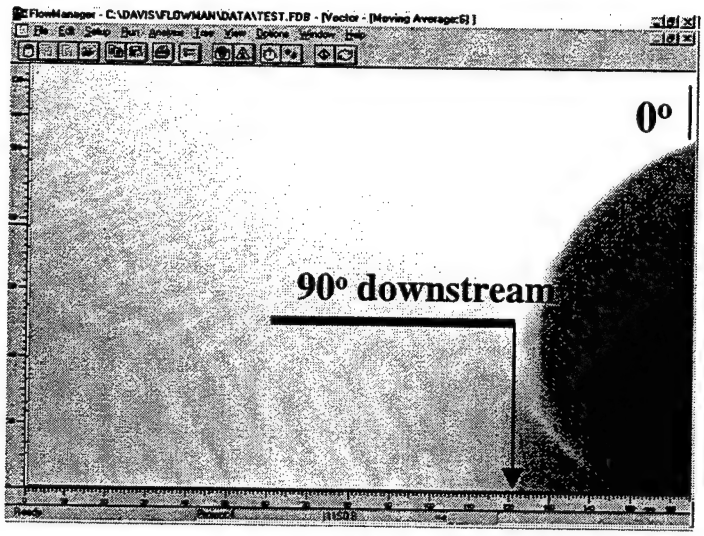

a)

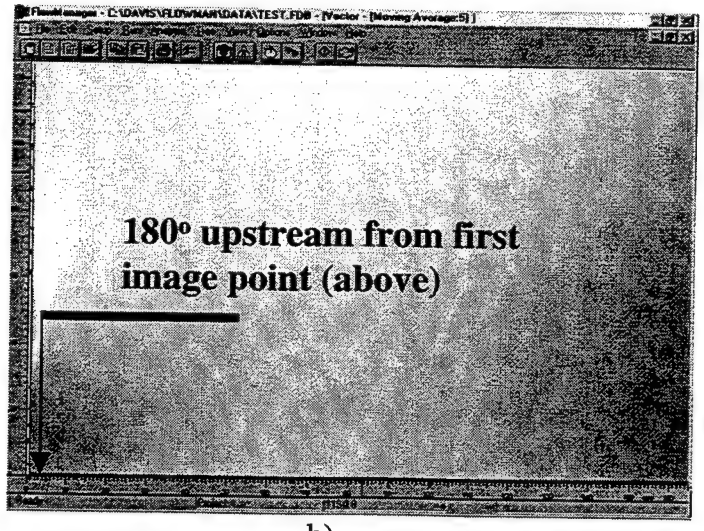

b)

FIG. 17. Cylinder displacement measurement technique when measurement point in first image can not be seen in second image.

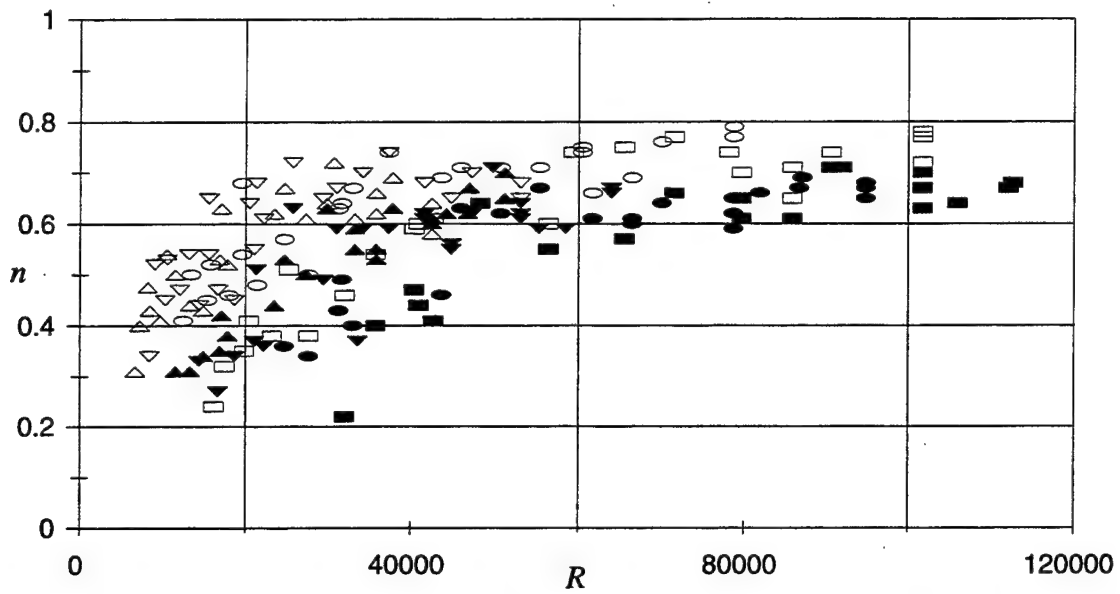

FIG. 18. Relationship between cylinder terminal velocity ratio and the Reynolds number for both the PIV and video-experiment results.

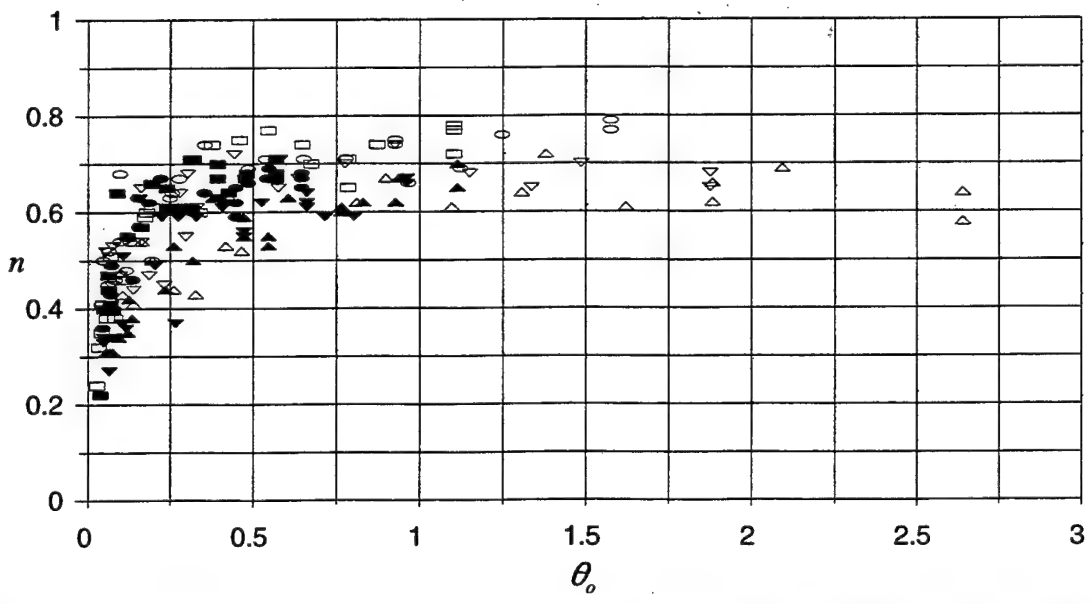

FIG. 19. Cylinder terminal velocity ratio and the modified Shields parameter for both the PIV and video-experiment results.

Establishing Steady-State Vector Fields

To see the characteristics of the flow around the cylinder, as if the coordinate system were fixed to the cylinder, the speed of the cylinder was subtracted from the measured vector field. This provided a steady-state image. Figure 20a shows the flow around a cylinder prior to subtracting the speed of the cylinder. Figure 20b shows the same data after the speed of the cylinder is subtracted from the vector field.

Rolling Cylinder Wake

During the PIV measurements, an experiment was conducted where the 0.115 m diameter steel cylinder was fixed in a flow of velocity 0.4 m/s. The cylinder neither rotated nor translated. The flow over the cylinder had separated from the cylinder creating a complex and varying flow field in the wake. Examples of the velocity fields downstream from the stationary cylinder are shown in Figs. 21a-c. The velocity fields in the figures were recorded one second apart. The flow patterns in Figs. 21a-c bear no resemblance to the flow patterns in the wake of rolling cylinders as shown for example in Figs. 20a-b. The many measurements of the flow field in the wake of rolling cylinders indicated that the flow does not separate from the surface of the cylinder which suggest that the wake could be considered two dimensional. This is an interesting result as Goldstein (1965) suggested that the aspect ratio (length to diameter) of a cylinder needs to be at least 20 to yield an effectively two-dimensional flow field downstream of a

stationary cylinder. Yet, the aspect ratios for the rolling cylinders in these experiments were less than 5.

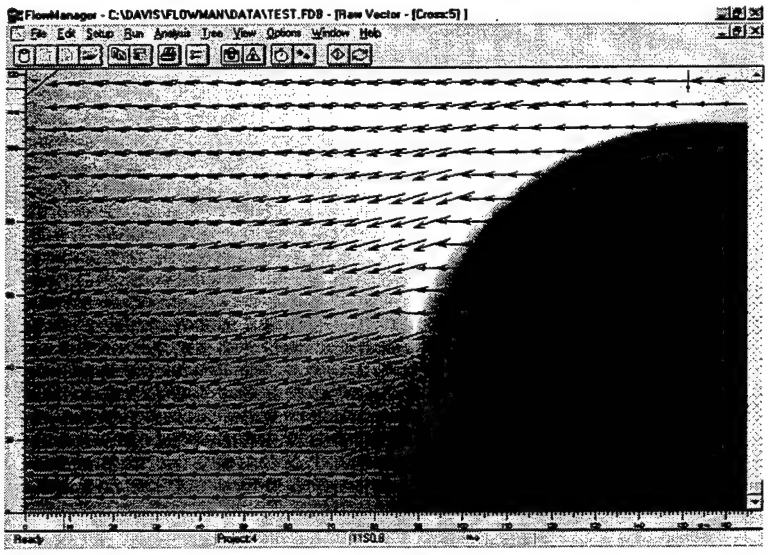

a)

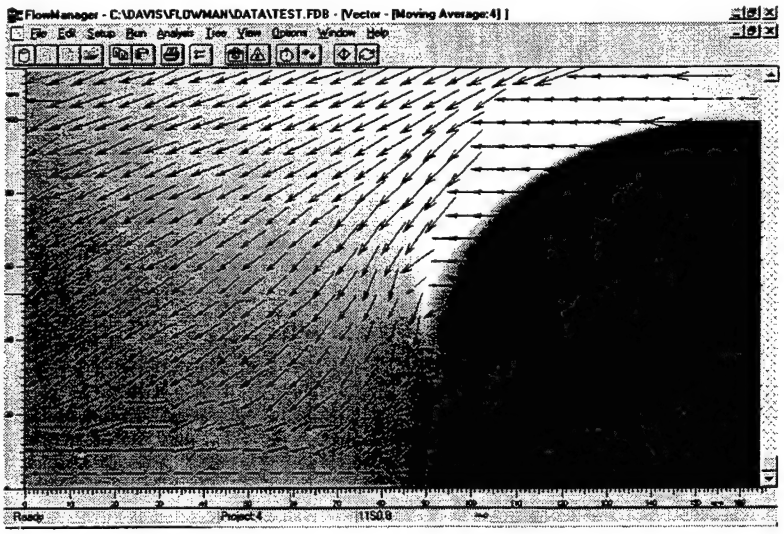

b)

FIG. 20. The flow field around a cylinder for the coordinate system fixed to a) the flume, and b) the cylinder.

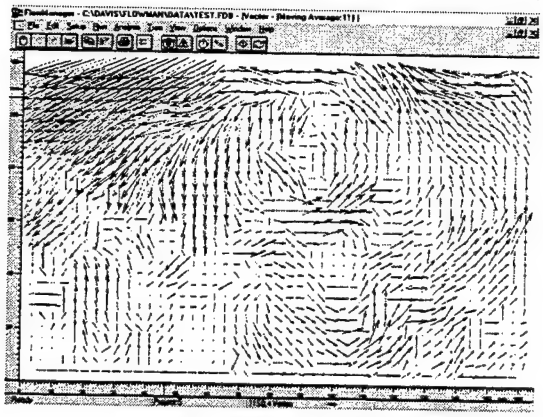

c) time = 3 seconds

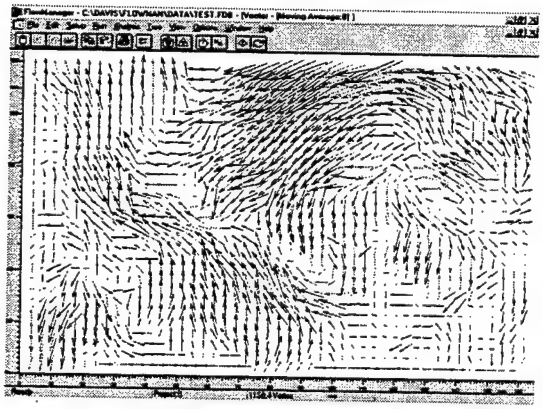

b) time = 2 seconds

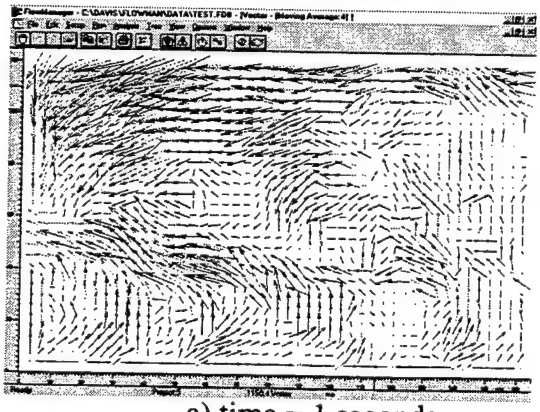

a) time = 1 seconds

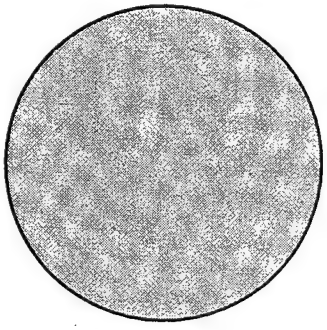

FIG. 21. Wake of the 0.115 m steel cylinder in a 0.4 m/s flow. Measurements of flow field were taken one second apart from (a) to (c).

To examine the character of a rolling cylinder's wake more closely, control-area calculations were made in the wake of the experimental cylinders. Recall that the net flow into a control area must be zero for incompressible fluids. Therefore, if the net flow into a two-dimensional control area placed in the wake of the cylinder is not zero, it would indicate the presence of a component of the flow perpendicular to the control area or that the flow is three-dimensional. The only certain statement that can be made from such an assessment though is that if the net flow into the control area is not zero, then a velocity perpendicular to the control area exists. However, in a practical sense, the approach outlined below provides a semi-quantitative means of establishing whether the wake is likely to be two- or three-dimensional.

Three types of flows were considered in the control-area assessment to gain an understanding of the dimensional character of the wake of rolling cylinders. First, control-area calculations were made in undisturbed flume flows (no cylinder present). This provided a measure of the ambient flow in the flume which is assumed here to be two-dimensional. The second set of control-area calculations was made in the wake region of the stationary, non-rotating cylinder shown in Figs. 21a-c. The flow downstream of the stationary cylinder is assumed to be three-dimensional because of its short aspect ratio as discussed previously. The third set of control-area calculations was made in the wake of the rolling cylinders.

To characterize the wake of a rolling cylinder, the control-area calculations from the wake of the rolling cylinders were compared to the control-area results for the ambient flume flow and the stationary cylinder to determine which they were most like. If the control-area results for the wake of the rolling cylinders were similar to the stationary-cylinder, then it could be assumed that the flow downstream of a rolling cylinder is three-dimensional. Conversely, if the control-area results for the wake of the rolling cylinders were similar to the ambient flume flow, the cylinder wake could be assumed two-dimensional.

A control area was used in the velocity fields from the PIV measurements as shown in Fig. 22. The PIV data contained the horizontal velocity component, u, and the vertical velocity component, v, for each vector. The vector spacing in a given direction was constant, so it was a straight-forward process to compute the flow across the control-area surfaces as $u\Delta y$ and $v\Delta x$, where Δx and Δy are the spacings in the horizontal and vertical directions, respectively. The flow into the control area in the horizontal direction was the sum of $u\Delta y$ at each grid point along the vertical sides of the control area. Similarly, the total flow into the control area in the vertical direction was the sum of $v\Delta x$ at each grid point along the horizontal sides of the control area. A positive value was assigned to flows out of the control area. The net flow in (q_i) and net flow out (q_o) of the control area were computed to obtain the value $e = [(q_o - q_i)/(q_o + q_i)]$ which was a measure of the error between the flow in and the flow out of the control area. This

formulation provided values between -1 and 1. If the error is negative more flow entered the control area than left, and if the error is positive more flow left than entered. The absolute value of the magnitude and the variability of the errors are the values compared between the three sets of control-area calculations.

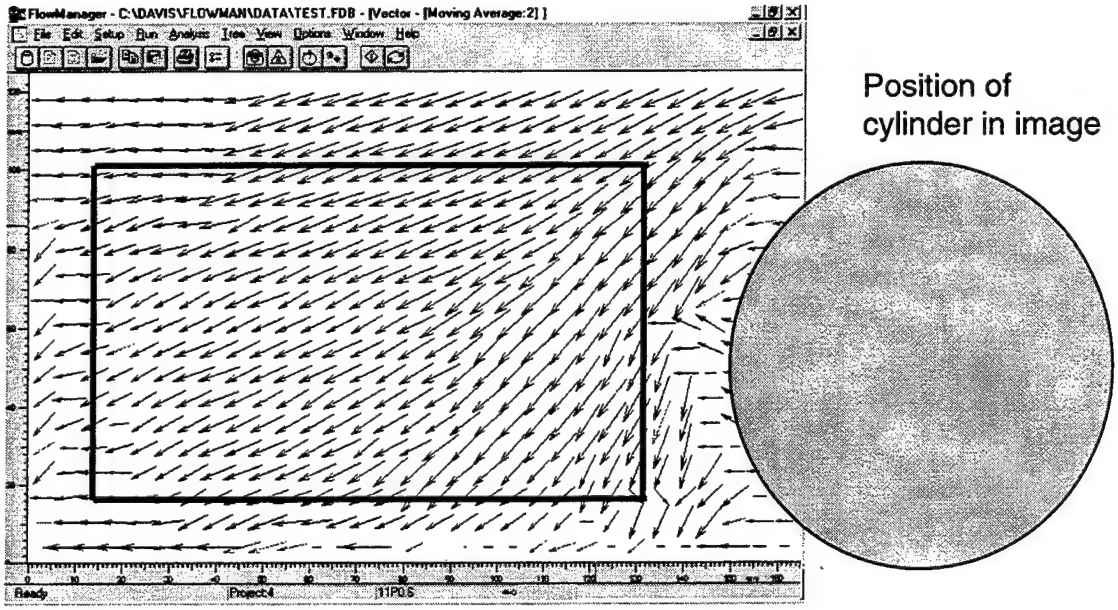

FIG. 22. Control area overlaid on a velocity vector field.

For the ambient flume-flow calculations, 33 of the PIV tests provided velocity vector fields that could be used. The value of *e* computed for the control areas in each of the vector fields are shown in Fig. 23. Most of the calculations resulted in values of *e* near zero. All calculated values were less than 0.10. The root mean square (RMS) was

0.04. For the wake region of the stationary cylinder, ten vector fields were available and all were used for the calculations. The results are plotted in Fig. 23. The values of e ranged between 0.16 to 0.65 with an RMS of 0.4. The ambient-flow and stationary-cylinder control-area calculations were considered indicators for the characteristics of the rolling cylinder wake. That is, if the values of e for the wake of a rolling cylinder are similar to those for ambient flow (RMS near 0.04) it would suggest that the rolling cylinder wake is two-dimensional. Similarly, values of e close to the stationary cylinder (RMS near 0.40) would suggest the wake is three-dimensional.

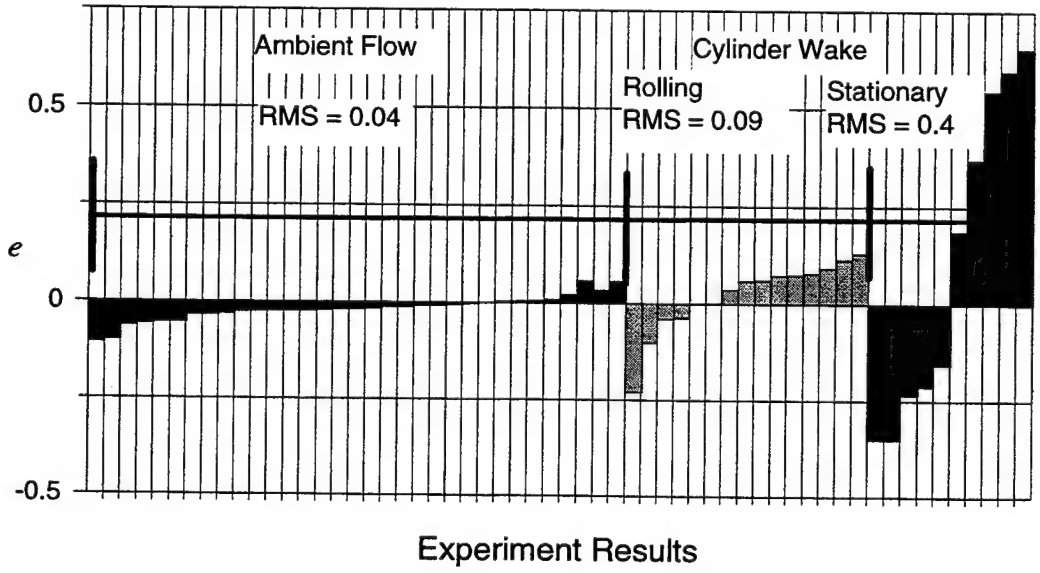

FIG. 23. Comparison between the net-flow errors computed from control areas in ambient flow fields, the wake of stationary cylinders, and the wake of rolling cylinders.

For the wake downstream of the rolling cylinders, 15 of the PIV tests provided velocity vector fields that could be used for the control area calculations. The calculated values of e are provided in Fig. 23. The values were less than 0.13 except for one which was 0.23. The RMS value was 0.09. Figure 23 shows that the magnitude of e was substantially smaller and the variation substantially less than the magnitude of e computed in the wake of the stationary cylinder. From this analysis, it could be concluded that the wake of a rolling cylinder is reasonably two-dimensional.

CHAPTER IV

INVISCID-FLOW THEORY APPLICATION*

Introduction

The results of the PIV measurements and the subsequent results of the control-area calculations discussed in Chapter III suggested that the flow around a rolling cylinder does not separate from the cylinder, and the wake of the cylinder is largely two-dimensional. The unseparated flow condition further suggests that the boundary layer may be confined to a thin layer of fluid near the cylinder's surface. This conclusion makes the application of inviscid-flow theory to describe the flow around the cylinder reasonable. To further simplify the inviscid flow derivations, the fact that the wake of a rolling cylinder is two-dimensional suggests that the cylinder in the inviscid flow derivation can be viewed as infinitely long in that the ends of the cylinder do not influence the flow in the wake. Hence, an inviscid-flow derivation for an infinitely long cylinder on a wall in a steady flow was used.

Derivation

Milne-Thomson (1968) provides an inviscid-flow derivation of the complex potential, w, for a cylinder on a bed in an inviscid, uniform, steady, and two-dimensional

*Parts of this chapter are reprinted with permission from "Terminal velocity of cylinders rolling in uniform flows" by Davis, J. E., Fenical, S. A., Zhang, J., and Edge, B. L., published in the *J. of Hydraulic Engineering*, September 1999, 125(9), 943-952. Copyright 1999 by the American Society of Civil Engineers (see Appendix II).

flow given by

$$w = a\pi U \coth\frac{a\pi}{z} \tag{4}$$

where a is the radius of the cylinder, U is the velocity of the free-stream flow and z is the complex variable, $x + iy$, where the origin for x and y is the contact point between the cylinder and the bed. (See also Mueller 1929.) Figure 24 provides a plot of the streamlines around the cylinder derived from Equation 4. The speed of the flow, q, is then given by

$$q^2 = \left(\frac{dw}{dz}\cdot\frac{d\bar{w}}{d\bar{z}}\right) = \frac{a^4\pi^4U^2}{r^4}\left(\frac{2}{\cosh\frac{2a\pi x}{r^2} - \cos\frac{2a\pi y}{r^2}}\right)^2 \tag{5}$$

which on the surface of the cylinder $r^2 = 2ay$ becomes

$$q^2 = \frac{a^2\pi^4U^2}{4y^2\cosh^4\left(\frac{a\pi x}{r^2}\right)} \tag{6}$$

where r is the distance from the origin and overbars on w and z indicate their complex conjugates.

Estimating the Terminal Velocity

The formulation for q can be used to estimate the terminal velocity of a rolling

cylinder. The approach assumes that the terminal velocity of the cylinder is achieved when flow separation is eliminated and that this condition occurs when the speed of the surface of the cylinder is everywhere equal to or greater than the speed of the inviscid flow around it. The speed of the flow around the surface of a cylinder on a wall is given by q. The speed of that flow depends on the free-stream velocity. The free-stream velocity relative to the cylinder depends on the speed of the cylinder. Hence, it is a straight forward process to find the speed of the cylinder that makes the speed of its surface everywhere equal to or greater than the inviscid flow around it. The derivation is outlined below.

The coordinate system must be attached to the cylinder which is accomplished by replacing U in Equation 6 with the relative free-stream velocity U_r given by

$$U_r = U_o - V \tag{7}$$

where U_o is the absolute free-stream velocity and V is the speed of the cylinder. To find the cylinder rotation that makes the speed of the cylinder's surface equal to or greater than the flow around it, V must equal or exceed the value for q everywhere around the cylinder's surface. From Equation 6, the maximum fluid velocity occurs at the top of the cylinder ($x = 0, y = 2a$) where $q = 2.46U_r$. Setting $V = q = 2.46U_r$, substituting Equation 7 for U_r, and solving for $n = V/U_o$, it is found that $n = 0.71$. In other words, when the

speed of the cylinder is 71% the speed of the free-stream flow, the speed of the cylinder's surface is everywhere as fast or faster than the fluid adjacent to it.

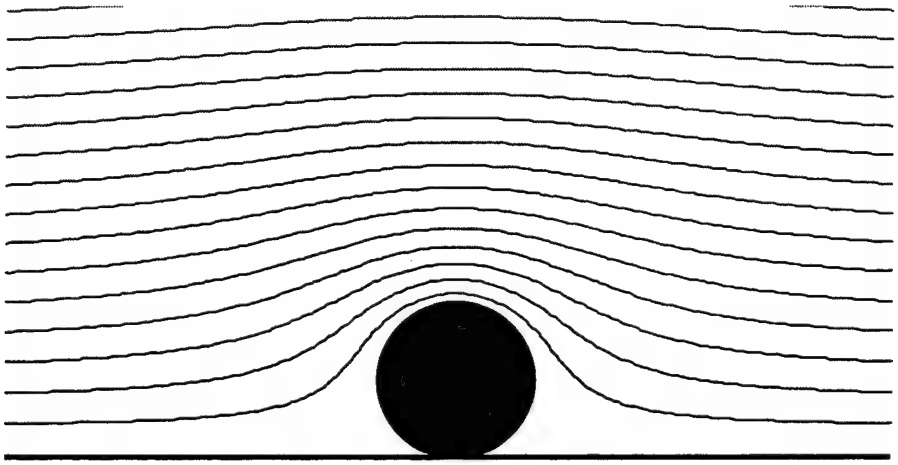

FIG. 24. Streamlines for a cylinder at rest on a wall in a potential flow.

This approximation for the terminal speed at which a cylinder will roll in a given steady, uniform flow included significant assumptions. The influence of the logarithmic portion of the velocity profile that exists near the bed is neglected; the generation of vorticity is neglected in regions where the speed of the cylinder's surface is different from the flow adjacent to it; the effect of the moving cylinder surface on the flow velocity around the cylinder is not considered; and the cylinder is assumed infinitely long such that the flow around it is two-dimensional. But, for all these assumptions, the laboratory experiments still gave a similar result for V/U_o.

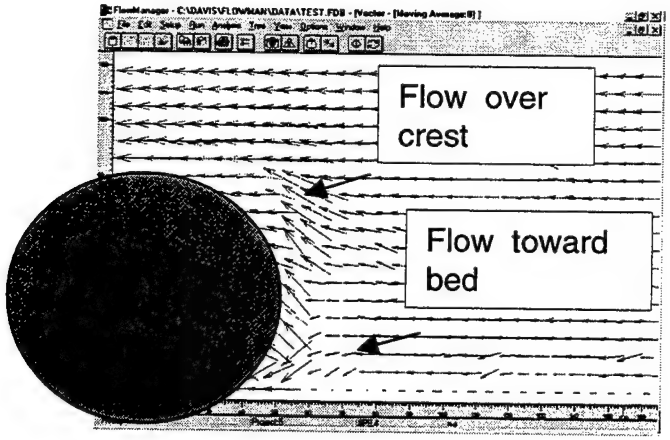

a)

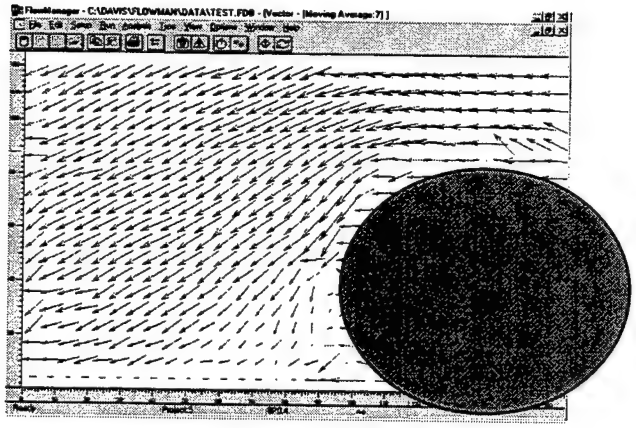

b)

FIG. 25. a) Flow is nearly horizontal on the upstream side of the cylinder except near the top and bottom of the cylinder. b) The flow is tangential to the cylinder surface on the downstream side similar to the inviscid-flow solution.

The most significant difference between the PIV velocity fields and those expected from inviscid flow theory is the asymmetry of the velocity field about the cylinder. Inviscid-flow theory applied to this problem results in symmetry about the vertical axis of the cylinder as seen in Fig. 24. In the experiments, however, on the

upstream side of the cylinders, the flow vectors are nearly horizontal close to the cylinder except near the top and sometimes near the bottom (Fig. 25a). On the downstream side of the cylinder, the flow vectors are tangential to the surface of the cylinder, more like those expected from inviscid-flow theory (Fig. 25b). Hence, the flow is not symmetric about the vertical axis of the cylinder. A flow pattern similar to the PIV results was observed in some of the numerical simulations for the upstream side of the cylinder. But on the downstream side, the flow pattern differed from both the experiment and inviscid flow results. The numerical investigation is discussed in Chapter V.

CHAPTER V

NUMERICAL SIMULATIONS

Introduction

The laboratory experiments described in Chapter III provided insights into the characteristics of the motion of rolling cylinders and the flows around them, but they did not provide information about the forces acting on the cylinders. The only inference of forces that can be made from the experiments is that when the cylinders reached their terminal velocities, the net force on the cylinders must have been zero. The inviscid flow derivations in Chapter IV can not be used to derive horizontal forces because the streamlines and pressures are symmetrical about the y-axis. Therefore, to address the issue of the forces acting on cylinders rolling at a given speed in a given flow, they were numerically simulated. The results provided the trends in forces for cylinders at different terminal velocity ratios, verified the terminal velocities observed in the experiments, and provided simulated velocity fields which could be compared to the PIV data. There were similarities between the PIV data and numerical results. Differences were also apparent as will be discussed below.

The numerical procedures and results are provided in detail in this chapter. A review of existing literature is also included. It is instructive to consider previous studies regarding forces on cylinders in flows. The literature is full of papers on the subject, but nearly all regard forces on restrained cylinders. While the studies reviewed here may not

directly apply to the present problem, they are nevertheless useful for gaining insights.

When a cylinder is at rest on a wall in a current, a drag force in the direction of flow and an upward lift force are exerted on it. The drag force F_D per unit length along a cylinder can be derived through dimensional analysis as

$$F_D = \frac{1}{2} C_D \rho U^2 D \tag{8}$$

where C_D is the drag coefficient which is a function of the Reynolds number, U is the free-stream velocity, D is the diameter, and ρ is the density of the fluid. A long, smooth cylinder in an unbounded, turbulent, free-stream flow has a drag coefficient of approximately 1.2. When the cylinder is on a wall, the drag coefficient is reduced. For example, Brown (1967) provides values ranging between 0.55 to 0.9, and Font (1967) provides values between 0.83 and 0.93 for flows with Reynolds numbers similar to those used in the experiments reported herein.

The lift force, F_L, can be written as

$$F_L = \frac{1}{2} C_L \rho U^2 D \tag{9}$$

where C_L is the lift coefficient. In contrast to the drag coefficient, the value of C_L is zero

away from the wall and has a theoretical limit of 4.49 derived from inviscid-flow theory while in contact with the wall (Wright and Yamamoto 1979). Prandtl and Tietjens (1957) also provided a theoretical limit on the lift coefficient of 4π for an infinitely long cylinder rotating in an unbounded, inviscid flow. This limit is achieved when the speed of the surface of the cylinder is four times the free-stream velocity of the flow past the cylinder. Subsequent work indicated that for real flows higher cylinder rotation rates can increase the lift coefficient well above Prandtl and Tietjen's theoretical limit (Thwaites 1960, and Tokumaru and Dimotakis 1993).

When a cylinder is moving in the flow, the appropriate velocity to use in Equations 8 and 9 is the relative velocity U_r between the flow and the speed of the cylinder (e.g. Lee and Hsu 1993, and van Rijn 1984). Therefore, as the speed of the cylinder increases, the relative flow velocity decreases, and so do the lift and drag forces.

If the cylinder is also rotating as it moves, the drag force may be reduced further as previously discussed. The work by Badr et al. (1990), and Tokumaru and Dimotakis (1993) showed for unbounded flows how rotating the surface of the cylinder influences the wake and can cause suppression of vortex shedding. They also noted that vorticity was generated on the bottom of the cylinder or the side of the cylinder moving in opposition to the free-stream flow. In the present problem, this location would be the contact point between the cylinder and the wall, so it is difficult to extrapolate their

results to this problem.

Previous work has shown that rotation will increase the lift on a cylinder (Goldstein 1965), but the magnitude of the lift on a cylinder due to rotation has a secondary effect compared to that due to the free-stream flow. Referring to spheres, Saffman (1965) stated that the influence of rotation on the lift force was an order of magnitude less than that due to steady flow past the sphere. While Saffman's work was for viscous flows, van Rijn (1984) reasoned that the same condition exists in turbulent flows. Based on observations from the laboratory experiments in this study, the same relationship may apply to cylinders. In the experiments at high flow velocities, the cylinders were lifted off the bed of the flume by the flow while attempts were made to hold them in place prior to their release indicating the lifting effect of steady flow past cylinders on a wall. Once the cylinders were released, however, they did not show any further tendency to lift off the wall. The decreasing relative flow past the cylinder decreased the lift force on the cylinder and was not compensated by the increasing lift due to the rotation of the cylinder.

The small aspect ratios of the cylinders used in the experiments had an undetermined influence on the drag and lift forces. Goldstein (1965) provides the drag coefficients for cylinders in unbounded flows for several aspect ratios. The values are reproduced in Table 5. The drag coefficient for an infinitely long cylinder is given by

$C_{D\infty}$. The table shows that the drag coefficients for cylinders are significantly reduced by small aspect ratios. A similar influence might be expected on the drag coefficient for a cylinder on a wall. The reduction in the drag coefficient is caused by the flows passing around the ends of the cylinder. However, as discussed in Chapter III and IV, the wake downstream of a rolling cylinder behaves more like a two-dimensional, unseparated flow. Hence, the reduction in drag for rolling cylinders due to small aspect ratios might be minimal.

TABLE 5. Drag coefficient aspect ratio for Reynolds number = 88,000 (after Goldstein, 1965).

L/D	∞	40	20	10	5	2.96	1.98	1
$C_D/C_{D\infty}$	1	0.82	0.76	0.68	0.62	0.62	0.57	0.53

Lift coefficients are reduced by small aspect ratios as well. Prandtl and Tietjens (1957) showed that the lift coefficients for small aspect-ratio, rotating cylinders in unbounded flows were increased by placing disks on the ends of the cylinders. The disks were twice the diameter of the cylinders and limited the end effects of the cylinder.

Simulations

In the laboratory experiments, no practical technique was available to instrument

the cylinders to measure the forces exerted on them. External or internal devices would have influenced the characteristics of the motion of the cylinder. The only available technique to evaluate the forces acting on the cylinder was numerical simulation.

The simulations described here modeled a cylinder rolling on a wall. The coordinate system was attached to the cylinder axis. Hence, the cylinder was stationary with respect to the grid. The speed of the cylinder surface was prescribed and the bed moved by at the same speed. Figures 26a and 26b compare the simulated velocities for a coordinate system fixed to the flume and one fixed to the cylinder, respectively. When cylinder speeds and flow velocities similar to the laboratory experiments were imposed in the numerical model, the numerical results supported the laboratory results. Namely, the simulations showed the elimination of flow separation and that the forces and moments acting on the cylinder were small.

Parameters within the range of the laboratory experiments were used in the numerical simulations. The Reynolds numbers in the simulations were based on cylinder diameters and free-stream velocities of the experiments. Terminal velocity ratios of $n = 0.6$, 0.71, and 0.8 were also used. In the simulations, a fixed two-dimensional cylinder was modeled. A relative flow velocity profile was input that was equal to the difference between the absolute free-stream velocity profile and the speed of the cylinder. (Refer to Figs. 26a and 26b.)

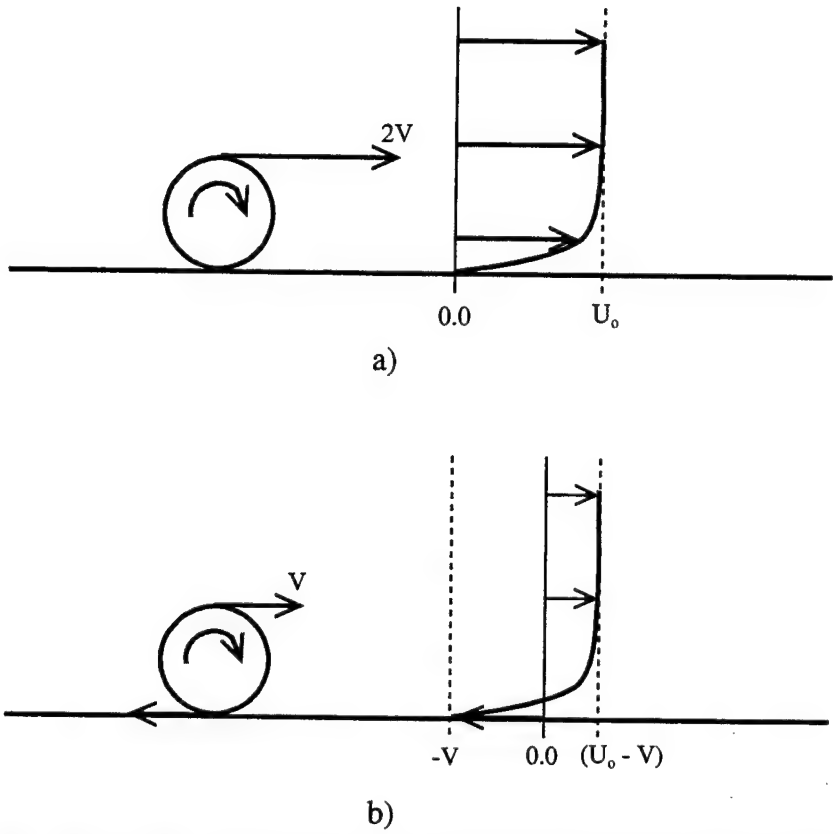

FIG. 26. Velocity profile and cylinder speed for a) coordinate system attached to the flume, and b) coordinate system attached to the cylinder.

The Numerical Model

The numerical model used for the cylinder simulations is documented by Chen, Patel and Ju (1990) and is discussed again by Hubbard (1994). It is a finite difference solution to the primitive governing equations for viscous, turbulent flow. The model is based on the Reynolds-Averaged Navier-Stokes (RANS) equations. The model uses a two-layer k - ε turbulence model. The equations are non-dimensionalized by the Reynolds number $R = U^* L^* / \nu$ where U^* and L^* are the characteristic velocity and length

chosen for the model and ν is kinematic viscosity of the fluid. For the simulations, the velocity of the free-stream flow and the diameter of the cylinder were chosen as the characteristic velocity and length, respectively. The governing equations used in the RANS code are discussed next. The code makes use of a chimera grid structure. Chimera grids and the grid chosen for this study are discussed later.

The RANS Flow Solver

In this study, turbulent flow is modeled using a Reynolds-Averaged form of the Navier-Stokes equations, or a RANS code. In the RANS code, turbulence is modeled using a two layer k-ε approach where a one-equation dissipation model is used for the viscous sublayer near solid surfaces and a two-equation model further out in the flow. The transport equations are based on the approach of Chen, Patel, and Ju (1990). The governing equations are described in this section.

The governing equations for viscous, incompressible flow are the continuity equation and momentum transport equations which in non-dimensional form are respectively:

$$\tilde{u}_i^{\,i} = 0 \tag{10}$$

and

$$\tilde{u}_o^i + \tilde{u}^j \tilde{u}_j^i + \tilde{p}_j - \frac{1}{R}\tilde{u}_{jk}^i = 0 \qquad (11)$$

where $\tilde{u}$ and $\tilde{p}$ are respectively the non-dimensionalized, instantaneous velocity and pressure. The subscript refers to differentiation with respect to the coordinate, i (j or k). The subscript o is differentiation with respect to time. The superscripts indicate the direction component being considered.

To convert these equations to the Reynolds-Averaged Navier-Stokes equations, the instantaneous velocity and pressure are decomposed into their mean and turbulent fluctuation components, or

$$\tilde{u}^i = U^i + u^i \qquad (12)$$

and

$$\tilde{p} = P + p \qquad (13)$$

where U and P indicate the mean values of the instantaneous variables, and u and p are the turbulent fluctuations about their respective mean. When Equations 12 and 13 are substituted into the Equations 10 and 11 and time averages taken, the equations yields

$$U^{i}_{i} = 0 \tag{14}$$

for the continuity equation, and

$$U^{i}_{o} + U^{j}U^{i}_{j} + (\overline{u^{i}u^{j}})_{j} + P_{j} - \frac{1}{R}U^{i}_{jk} = 0 \tag{15}$$

as the transport equations.

Reynolds averaging results in an additional tensor containing the time-average of the product of the turbulent fluctuations. These terms are called Reynolds shear stresses as they appear to function like the viscous shear stress terms in the Navier-Stokes equations. Since the turbulent fluctuations are correlated, their time average will not necessarily be zero. Hence, nine new terms enter the governing equations, but only six new unknowns are added because of the tensor is symmetric.

Because there are too few equations to solve for the unknowns, several models for the Reynolds stress terms have been developed. The method used in this RANS code is the k -ε model where the turbulence kinetic energy, k, and its dissipation rate, ε, are modeled. The approach expresses the increase in shear due to turbulence in terms of an "eddy" viscosity, ν_t, akin to the influence of molecular viscosity in the viscous shear stress terms. The Reynolds stresses are written in terms of the eddy viscosity and the

mean flow properties as

$$-\overline{u^i u^j} = \nu_t \left(U^{\,i}_{\,j} + U^{\,j}_{\,i} \right) - \frac{2}{3} k \delta_{ij} \tag{16}$$

where k is further defined by

$$k = \frac{1}{2} (\overline{u^i u^i}) \tag{17}$$

and δ_{ij} is the Kronecker Delta Function. The turbulence kinetic energy and its dissipation are related via the eddy viscosity by

$$\nu_t = C_\mu \frac{k^2}{\varepsilon} \tag{18}$$

where C_μ is a fixed constant equal to 0.09. Transport equations for both k and ε are used in the model. Therefore, the five coupled equations for U^i, k, and ε along with the continuity equation are available to solve for the six unknowns, namely U^i, P, k, and ε.

A sometimes-limiting assumption of the k - ε turbulence model is that turbulence is isotropic. For many flow situations, this is a valid assumption. But near a wall or other boundary, turbulent fluctuations can be damped in the direction normal to the wall making the turbulence anisotropic. For these problems, the RANS code uses a two-layer

approach. In the region or layer away from the wall, the full k - ε approach is used. Near the wall, the dissipation rate of k is defined by the magnitude of k and a dissipation length scale which is a function of the proximity of the wall.

The Chimera Grid and Grid Generation

The RANS code used in this study takes advantage of chimera grids for the solution domain. A chimera grid uses an assemblage of structured meshes to create a complete and optimal grid for the flow. A flow domain can sometimes be decomposed into simple geometric regions and flow meshes generated for each. They may then be combined into one complete solution grid. In complicated flow regions, higher mesh resolution can be inserted without having to increase the resolution of all of the meshes. In cases where objects are moving through the flow, the meshes can be designed to minimize the amount of grid-regeneration necessary. As an object and its boundary meshes move during a simulation only the coordinates of the moving-mesh nodes and their connectivity with the other stationary meshes are recomputed. This approach is computationally less intensive than regenerating the entire solution grid at each time step (Hubbard 1994).

For this problem, the chimera-grid technique was selected because it offered a simple approach to generate the solution grid which was a combination of circular and rectangular meshes. A cylindrical mesh was used around the cylinder and a rectangular

background mesh was used for the ambient flow. Near the contact point between the cylinder and the wall, a highly refined rectangular mesh was added to improve computations in that complicated flow region. The combined meshes are shown schematically in Fig. 27. While other grid techniques were viable for a cylinder resting on a wall, the option was left open to simulate the movement of a cylinder across the solution grid. Therefore, the chimera-grid technique was considered the best choice for this study. In the end, it was not necessary to have a cylinder moving across the solution grid, but the chimera technique used here was still sufficient to study the relative motion of the fluid (and wall) past the cylinder.

The solution on a chimera grid proceeds from one mesh to another as information is passed back and forth between meshes by interpolation. Along the overlapping edges of meshes, *boundary points* are identified to receive information from their adjacent meshes and *interpolation points* are identified to send information to adjacent meshes. Interpolation points in a mesh surround boundary points on another mesh. Together, the interpolation points form an *interpolation stencil* for the boundary point. Information is transferred to the boundary point by interpolating values from the interpolation stencil. Developing interpolation stencils for all of the meshes and boundary points was accomplished with PEGSUS, a program developed by Suhs and Tramel (1991) for chimera grids.

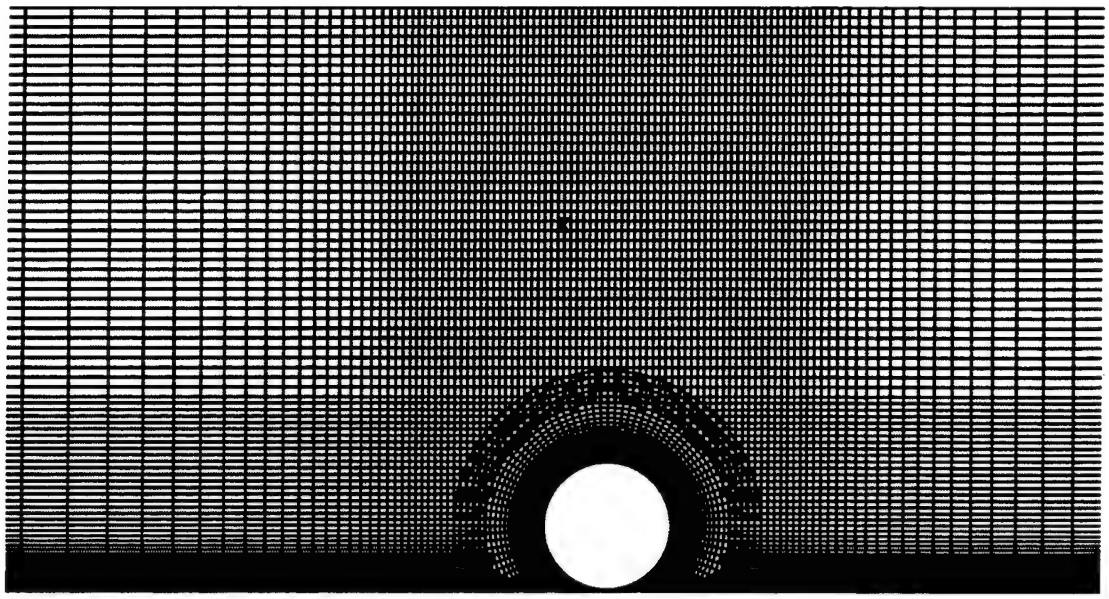

FIG. 27. Combined meshes in solution grid.

PEGSUS Program

PEGSUS is used to generate the interconnections between meshes in the computational grid. Besides the boundary points and interpolation stencils mentioned, PEGSUS also identifies field points, hole points, and hole-boundary points. *Field points* are away from the boundary of the mesh and are not included as boundary points or used in interpolation stencils. *Hole points* are points that need to be taken out of the computational domain. Hole points occur, for example, when grid points on an overlapping mesh fall within the boundaries of a solid object. Those points are identified as hole points and no flow computations are made with them. Essentially, the solid

object makes a *hole* in the overlapping mesh. The points laying between hole points and field points in a mesh are called *hole-boundary* points. Hole-boundary points receive information from adjacent meshes to insure continuity across the mesh.

Grid features that create hole points in meshes are specified in PEGSUS as boundaries. When grid points are located on the *inside* of a specified boundary such as the surface of the cylinder or the bed, they are labeled hole points and are removed from the computational domain. A normal vector pointing "out" of the boundary is defined by the user which allows PEGSUS to determine whether points from an overlapping mesh fall inside or outside of the specified boundary.

When PEGSUS is unable to identify a sufficient number of interpolation points to make a stencil for an adjacent mesh boundary point, that boundary point is labeled an *orphan*. If an orphan is created no information can be interpolated to it. This may create problems during the simulation. So, it is important to correct meshes to eliminate orphans. The overlap between meshes must be sufficient to ensure that a complete interpolation stencil can be found for each boundary point. To facilitate finding good interpolation stencils, it is helpful for the grid spacing to be similar between adjacent meshes in the region of overlap and for the overlap area to be several cells in width. In the meshes for this problem, the grid dimensions in the overlap regions were nearly the same, see for example, Fig. 28.

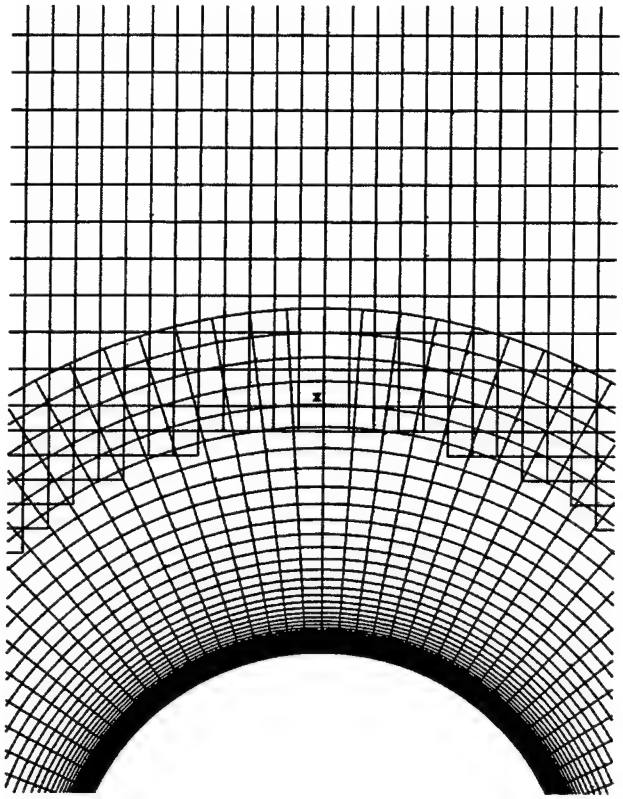

FIG. 28. Overlapping cylindrical and rectangular mesh cells are of nearly equal size.

In the meshes near the point of contact between the cylinder and the bed, several problems were encountered though eventually resolved. This is a region where meshes have to reduce to a single point. Short of creating a mesh that matched both the bed and cylinder boundaries and collapsed to a single node at the contact point, every grid combination tested produced orphan points. The solution to the problem was to allow a small gap to exist between the cylinder and the bed. In this way, a sufficient number of points could always be found to create interpolation stencils. The gap used was 1/100 the

diameter of the cylinder (Fig. 29).

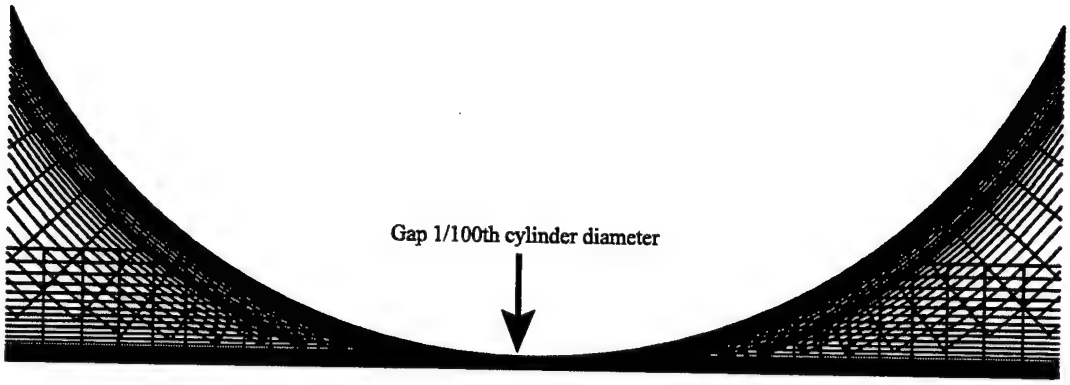

FIG. 29. Small gap used to avoid creation of orphan points in solution grid.

As input, PEGSUS requires the coordinates of all grid points in all meshes. The user must also instruct the program as to which meshes are linked, i.e. which transfer information to one another across their boundaries. When a mesh is linked to several other meshes, the user must also specify the mesh priority for PEGSUS as it selects meshes to build interpolation stencils for boundary points. Any boundaries that create holes in any overlapping meshes must be specified (e.g., the surface of a solid object). Other specifications are possible with PEGSUS, but those listed above were the most significant features used in this investigation.

Grid Generation

Several mesh configurations were tried in this study and the meshes described here were ultimately selected because they did not produce orphan points or instability throughout most of the computations. The general computational grid was 10 cylinder diameters from inlet to outlet and 4.5 diameters from the bed to the top of the grid. (Note the diameter of the cylinder was selected as the length scale in the computations and all length dimensions are therefore given in terms of cylinder diameters unless otherwise specified.) The coordinate system used in the study was attached to the cylinder with the point (0,0) at the cylinder's center. The bottom of the cylinder was located 1/100th of a diameter above the lower grid boundary. The lower boundary was therefore located at y = -0.51. The inlet of the solution grid was at x = -5.5. The solution grid is shown schematically in Fig. 27.

The grid spacing was finest near the solid boundaries to adequately resolve the boundary layer in those regions. The heights of the cells at the solid boundaries were defined by

$$y^+ = \frac{y u_*}{\nu} \leq 5 \tag{18}$$

where y^+ is the nondimensional cell height required to resolve turbulence dissipation; u_* is the shear velocity at the boundary which for the design of the grid was assumed equal

to 0.04 m/s for estimation purposes based on smooth, flat plate values; and ν is the kinematic viscosity of the fluid taken as 10^{-6} m^2/s. Solving for the dimensional height of the cell, y, yields $y \leq 0.000125$ m. When non-dimensionalized by cylinder diameter, the required non-dimensional cell height becomes ≤ 0.00125 diameters (0.1 m was used to approximate the diameter of the experimental cylinders). To reduce the occurrence of stability problems, the actual cell thickness used was 0.0001 diameters. Twenty grid cells were used to define the viscous sublayer which was assumed to extend to $y^+ = 100$-300. A value of $y^+ = 120$ was used which implied the outer edge of the viscous sublayer was at 0.03 diameters from the surface.

The inner-most cells in the viscous sublayer had a thickness of 0.0001 diameters that expanded to 0.005 diameters in the outer-most cells. A stretching function was used to calculate a reasonable expansion rate in cell size between the wall and the outer portion of the sublayer. The function was developed by Vinokur (1980). Vinokur's approach uses a function based on the inverse tangent that yields specified gradients in spacing at both ends of a given interval. A modification of Vinokur's approach was used in this study where the desired grid spacings on either end of the interval are specified rather than the gradient. Vinokur's algorithm is then used iteratively to find a solution that yields the desired grid spacing

Four meshes were used to create the computational grid. A rectangular

background mesh named "BCKGRND" was used as the inlet and outlet for the flow. Around the cylinder, cylindrical meshes were used. One mesh named "TOPCYL" was used for the top half of the cylinder and one mesh named "BOTCYL" was used for the bottom of the cylinder. In addition, a mesh called "CONTACT" was used to create a refined mesh in the region of the contact point between the cylinder and the wall. As mentioned, a small gap was used between the cylinder and the wall to ensure interpolation stencils could be found for all boundary points in the vicinity of the contact point. The small gap between the cylinder and the bed created a slightly different flow condition in that region than would have existed if the cylinder was actually in contact with the bed. However, the effect was confined to the region very near the contact point and did not influence the general flow around the cylinder.

Characteristics of BCKGRND

The background mesh contained the inlet and outlet boundary conditions for the computations and the boundary conditions for the bed. A specified velocity profile was introduced at the inlet adjusted as shown in Fig. 26 and described later in this section. At the outlet and top of the grid a zero-gradient boundary condition was imposed. On the bed, a no-slip condition was imposed. The velocity of the bed was specified. Twenty grid cells were used for the viscous sublayer (described previously) and ranged from y = -0.51 to -0.48 diameters. From y = -0.48 to +0.5, 35 grid points were used with cell thicknesses expanding from 0.005 nearest the wall to 0.05 furthest away. Ten additional

cells of constant thickness 0.05 were used between $y = +0.5$ to $+1.0$; and 40 cells were used of constant thickness 0.075 from $y = +1.0$ to $+4.0$. Horizontally, 25 grid cells were used to vary the width of the cells from 0.5 at $x = -5.5$ (at the inlet) to 0.05 at $x = -1.5$. Sixty cells of constant spacing 0.05 covered the region between $x = -1.5$ to $+1.5$. Another 21 cells were used to expand the downstream cells identical to the upstream spacing. Horizontally, the grid was symmetrical about a vertical plane at $x = 0.0$ except that the outer limits of the grid were truncated on the downstream end to optimize computation time. The grid is shown if Fig.30.

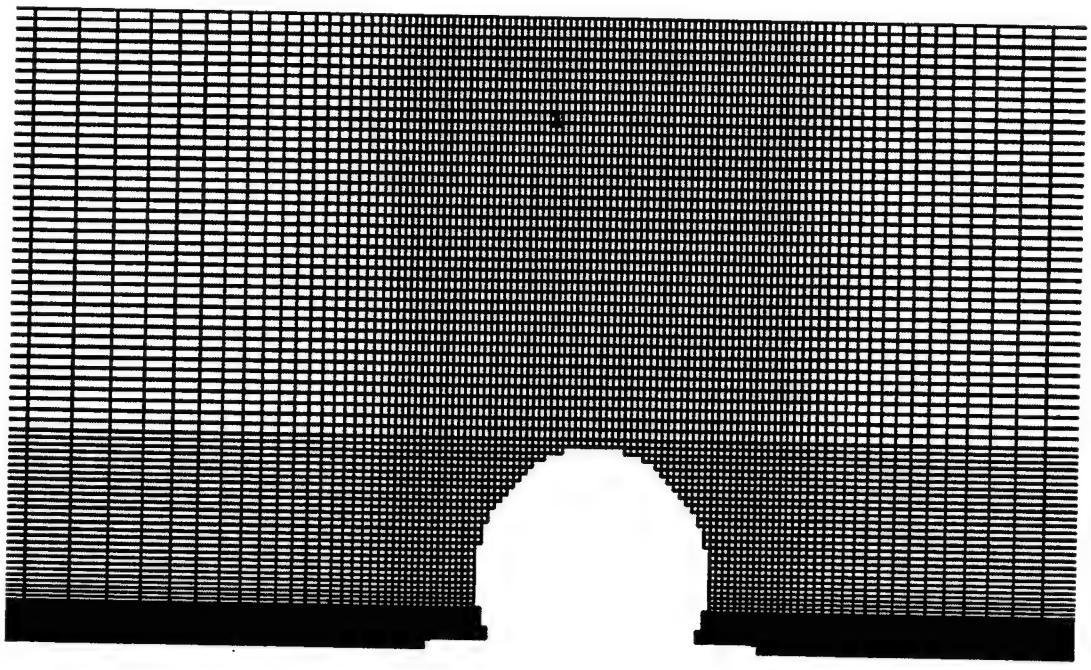

FIG. 30. Background rectangular mesh. The empty region at the center and bottom of the mesh is a hole created by in the TOPCYL, BOTCYL, and CONTACT meshes.

Characteristics of TOPCYL and BOTCYL

The cylindrical meshes located around the top and bottom of the cylinder were identical. In these meshes, the x-direction is circumferential around the mesh and the y-direction is radial. The grid cells nearest the surface of the cylinder were defined as described above for the viscous sublayer. An additional 31 cells were used to extend the mesh from the edge of the sublayer to a point 0.75 diameters from the cylinder surface. These cells ranged in thickness 0.005 at the edge of the sublayer to 0.05 at the edge of the mesh. The thickness of the cylindrical mesh cells and background mesh cells were approximately the same in the overlapping regions. The width of the cells were defined by radial lines spaced 0.02π apart. The boundary grid points in the top mesh, TOPCYL, were made to exactly match the grid points in the bottom mesh, BOTCYL, so that overlap could be reduced to one cell thickness. No interpolation of data from one mesh to the other was needed as the grid points corresponded one to one. The meshes are depicted in Fig. 31.

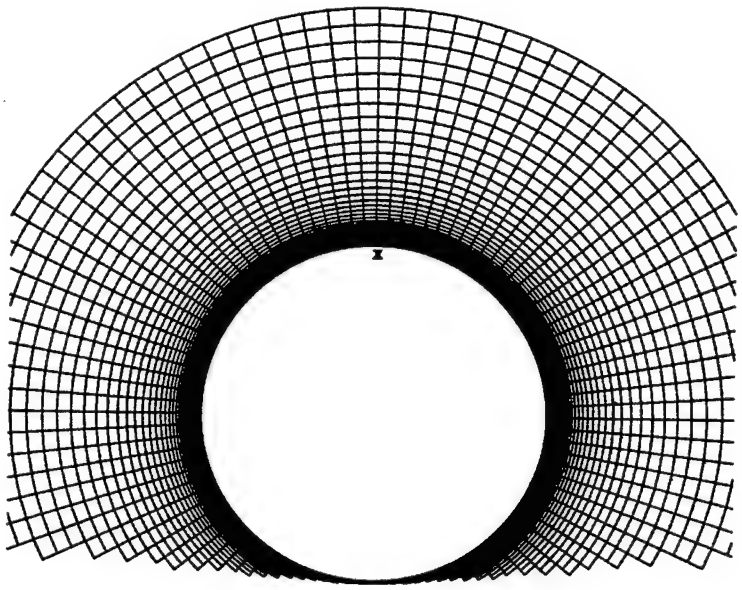

FIG. 31. Circular meshes that surround cylinder. The wall makes a hole in (or truncates) the lower portion of mesh.

Characteristics of CONTACT

The width of the mesh refining the region around the contact point between the cylinder and bed ranged between y = -0.51 and 0.0. The length of the mesh ranged between x = -1.55 and +1.55. The vertical spacing of the mesh was identical to the background mesh. The horizontal spacing between x = -1.55 to -0 .005 ranged respectively from 0.05 to 0.005 diameters over 50 cells. The mesh was symmetrical about the vertical axis at x = 0. The mesh is depicted in Fig. 32.

FIG. 32. Rectangular mesh used to refine the region near the contact point between the wall and the cylinder.

Creating Holes in Meshes

The solid area of the cylinder made a hole in the BCKGRND (Fig. 30) and CONTACT (Fig. 32) meshes and the bed made a hole in a portion of BOTCYL as shown in Fig. 31. The hole in BCKGRND and CONTACT was determined by defining the surface of the cylinder as a boundary in the BOTCYL and TOPCYL meshes. The inside edge of the meshes defined the boundary (or cylinder surface). The hole in BOTCYL was created because the outer portion of this mesh fell below the bed which was defined as the "inside" of the bed boundary.

Simulation Methodology

A two-dimensional solution was obtained in the numerical investigations. This implied that the cylinder was infinitely long and that the flow around it was two-dimensional. While the flow characteristics around the finite-length laboratory cylinders

may have been three-dimensional, the PIV results suggested that the three-dimensional aspect was weak and that flow might be reasonably considered two-dimensional. (See Chapter III.) During the numerical simulations, it was difficult to achieve stable solutions for all of the R and n combinations tried probably due to the grid resolution used. Future research should consider other types of grid formulations that could yield stable solutions for all combinations of R and n. Three-dimensional solutions for the same cylinder simulations studied here should be pursued, as well as simulations of cylinder motion beginning from rest.

In the two-dimensional simulations, an inlet velocity profile was specified on the inlet side of the grid. The profile for the simulation was found by running a constant velocity (1.0) at the inlet (no boundary layer). At a distance downstream from the inlet, the development of the boundary layer near the wall was evident. The simulation was stopped, the new velocity profile extracted from the solution and reintroduced at the inlet for additional simulation. This process was repeated until an unchanging velocity profile was achieved. The final profile shape used in the simulations is compared in Fig. 33 with example PIV experiment data. The velocity profile compares well with those measured in the experiments discussed in Chapter III. This profile was the input profile used throughout the simulations. The inlet was set five diameters upstream from the cylinder to allow the profile to adjust to the simulated conditions.

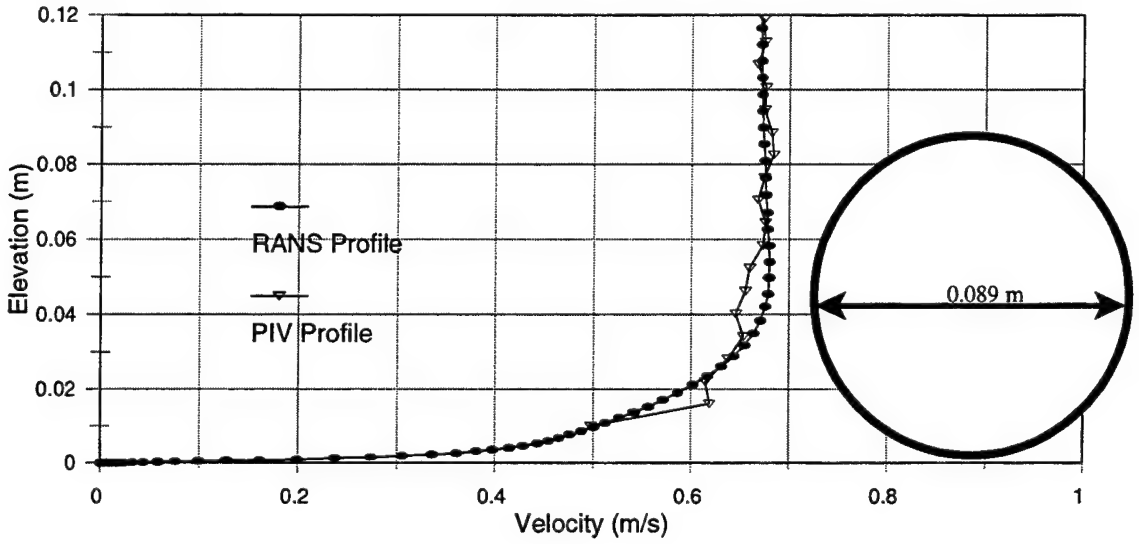

FIG. 33. Velocity profile used in the numerical simulations compared with a velocity profile from the laboratory experiments.

The approach used for the simulation was to fix the coordinate reference frame to the rolling cylinder so that the cylinder remained stationary while its surface rotated and the bed moved past the cylinder at the same speed. The inlet velocity profile had to be adjusted for the change in the coordinate reference frame. This was done by subtracting the speed of the cylinder from the magnitude of the profile velocities. This process was depicted in Figs. 26a-b. In this modified profile, the upper portion of the profile has fluid moving downstream past the cylinder while near the wall it is moving upstream.

The bed and the surface of the cylinder in the simulation were assigned the speed

of the cylinder. In conjunction with this, a no-slip condition was enforced on both surfaces to ensure that the speed of the fluid in contact with a surface was always moving at the speed of the surface.

Solution Convergence Time

The simulations were executed on the Silicon Graphics, Inc., Origin 2000 computer system located at the US Army Engineer Research and Development Center in Vicksburg, MS. The Origin 2000 has 112 processors, though for these simulations only one processor was used. The system has 64 Gbytes of memory and ½ Tbytes of harddisk storage space. The peak computational capacity of the system is 49.9 GFlops. The simulations normally required 6000-10,000 time steps to converge on a steady-state solution where convergence was defined as unchanging total forces on the cylinder. Generally, 2000 time steps were completed each day. Therefore, one week per simulation was required given that no problems were encountered during the simulation.

Simulation Results

Forces and Moments on the Cylinder

The forces and moments on the cylinder were derived from computed normal pressures and surface shear stresses. The forces are presented here as the downstream directed force C_x and the total upward directed force C_y. The moment C_m about the contact point between the cylinder and the bed was also computed. A positive moment

resisted rolling while a negative moment induced rolling. The forces are considered positive in the downstream and upward directions. All of the forces and moments are given in non-dimensional form.

The pressure was computed for each surface grid point. The pressure multiplied by the discrete surface area, Δs, over which the pressure acted gave a normal surface force. Geometry was then used to derive the component form of the force. The horizontal and vertical components of the pressure-induced force are respectively given by C_{xp} and C_{yp}. Similarly, the forces induced by the surface shear stresses were computed. The horizontal and vertical components of the shear-induced force are given respectively by $C_{x\tau}$ and $C_{y\tau}$. The moments about the contact point were computed from the incremental pressure- and shear-induced forces around the surface of the cylinder multiplied by the appropriate moment arm. The moments induced by the pressure and shear forces are given respectively by C_{mp} and $C_{m\tau}$. The resulting total forces and moments for each simulation are given in Table 6 with respect to the Reynolds number and the cylinder terminal velocity ratio (n).

TABLE 6. Computed forces and moments on cylinders.

R	n	C_{xp}	$C_{x\tau}$	C_x	C_{yp}	$C_{y\tau}$	C_y	C_{mp}	$C_{m\tau}$	C_m
14000	0.71	-0.027	0.003	-0.025	0.090	-0.001	0.089	0.018	0.007	0.020
27000	0.60	0.033	0.003	0.036	0.194	0.001	0.194	-0.017	0.003	-0.013
	0.71	0.003	0.002	0.005	0.047	-0.001	0.046	-0.002	0.006	0.004
	0.80	-0.021	0.002	-0.019	-0.003	-0.002	-0.005	0.011	0.007	0.018
52000	0.71	0.010	0.003	0.013	0.040	-0.001	0.039	-0.005	0.005	-0.000
	0.80	-0.011	0.001	-0.010	-0.008	-0.002	-0.009	0.006	0.006	0.011
72000	0.71	-0.000	0.001	0.001	0.022	-0.001	0.021	0.000	0.005	0.005

The total horizontal forces and the moments in Table 6 are plotted in Fig. 34. The results are consistent with the results of the laboratory experiments in that at low Reynolds numbers (e.g., R = 14,000), the cylinder rotating at $n = 0.71$ has an upstream directed force and moment acting on it, i.e. slowing it down. The experimental data indicated that at low Reynolds numbers the cylinders rolled at $n < 0.70$ (Fig. 18). A reason given for the experimental results falling below $n = 0.70$ was resistance of the cylinders to roll due to their submerged weight (recall the discussion and use of the modified Shields parameter). However, the mass of the cylinders was not required in these simulations. Therefore, at low Reynolds numbers, the characteristics of the flow itself must have an influence on the terminal velocity of the cylinders. As the Reynolds

number increased to 27,000, the moment on the cylinder rotating at $n = 0.71$ approached zero indicating that the cylinder was at or near an appropriate value of n for that condition. The downstream directed forces were also slightly positive which may be necessary to overcome rolling resistance (e.g., friction at the bed). Resisting forces at the bed, however, do not influence the calculation of the moment about the contact point. Contrast these results for $n = 0.71$ to those for $n = 0.6$ and 0.8 where the forces and moments would accelerate and decelerate the cylinders, respectively.

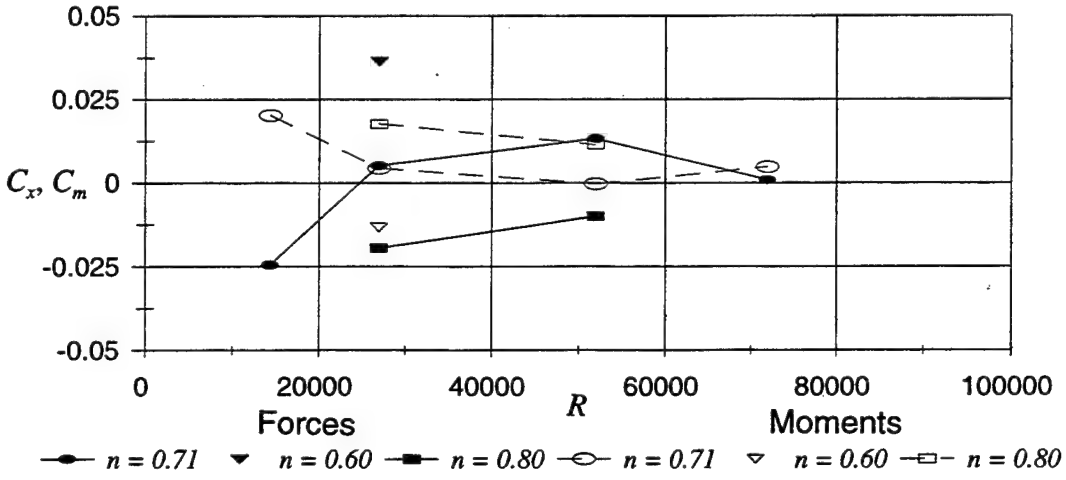

FIG. 34. Computed horizontal forces and moments about contact point.

At $R = 52{,}000$ and $n = 0.71$, moment is still virtually zero while the force acting on the cylinder has increased slightly in the downstream direction. The cylinder rolling at $n = 0.80$ continues to have a resisting force and moment acting on it. That is, the

cylinder would be decelerated. A solution could not be obtained for $n = 0.6$ at higher R values with the given grid. Lower R values were not simulated.

At $R = 72{,}000$ and $n = 0.71$, both the moment and force on the cylinder remain near zero. A solution for the case of $n = 0.8$ could not be obtained with the given grid. It should be noted as well that at $R = 84{,}000$ a solution could not be obtained for $n = 0.71$ with the given grid. The numerical results presented above suggest that cylinders rolling under two-dimensional flow conditions will reach their terminal velocity ratio at about $n = 0.7$, since the moment about the contact point is essentially zero.

The lift on the cylinder was greatest for the case where $n = 0.6$ as shown in Fig. 35. For all R conditions simulated, the lift was positive for $n = 0.71$ and slightly negative for $n = 0.80$. A slightly decreasing lift could be seen for both $n = 0.71$ and 0.8 as R increased from 27,000 to 72,000. The decrease in lift for $n = 0.71$ between $R =$ 14,000 and 27,000 was more substantial.

Flow Patterns

While simulated forces and moments on the cylinders were consistent with experimental results, the simulated flow patterns around the cylinder differed from most of the flow patterns measured during the experiments. In the simulation, prominent flow characteristics were observed on the upstream and downstream sides of the cylinders that

were not observed (or at least were not as pronounced) in the experiment data. These differences as well as the similarities are discussed below. The flow patterns were similar for the various combinations of n and R. The case for $n = 0.6$ and $R = 27{,}000$ is presented first in detail. Only the notable differences between this condition and the conditions for $n = 0.7$ and 0.8 are discussed afterward.

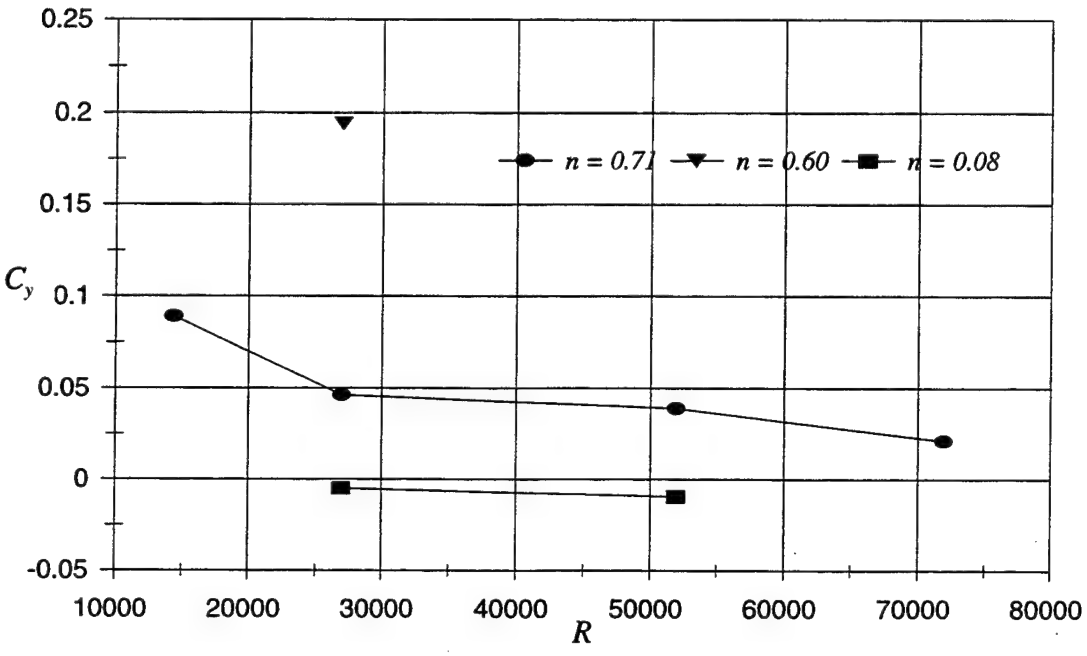

FIG. 35. Computed lift forces on the cylinder.

On the upstream side of the cylinder, for the simulated case $n = 0.60$, and $R = 27{,}000$, the flow "stagnation streamline" would terminate just below the horizontal

axis through the center of the cylinder. The "stagnation streamline" does not actually terminate on the surface of the cylinder since the surface of the cylinder is moving. Rather, it is considered the line above which flow is directed over the crest of the cylinder and below which flow is directed toward the bed as shown in Fig. 36. For this condition, a vortex appeared on the upstream side of the cylinder near the wall reminiscent of the "separation bubble" described by Fredsøe and Hansen (1987) that formed on the upstream side of a cylinder in contact with a wall. A clearly visible vortex was observed in a few of the PIV measurements, an example of which is shown in Fig. 37. In most of the PIV results, a flow directed toward the bed just upstream of the

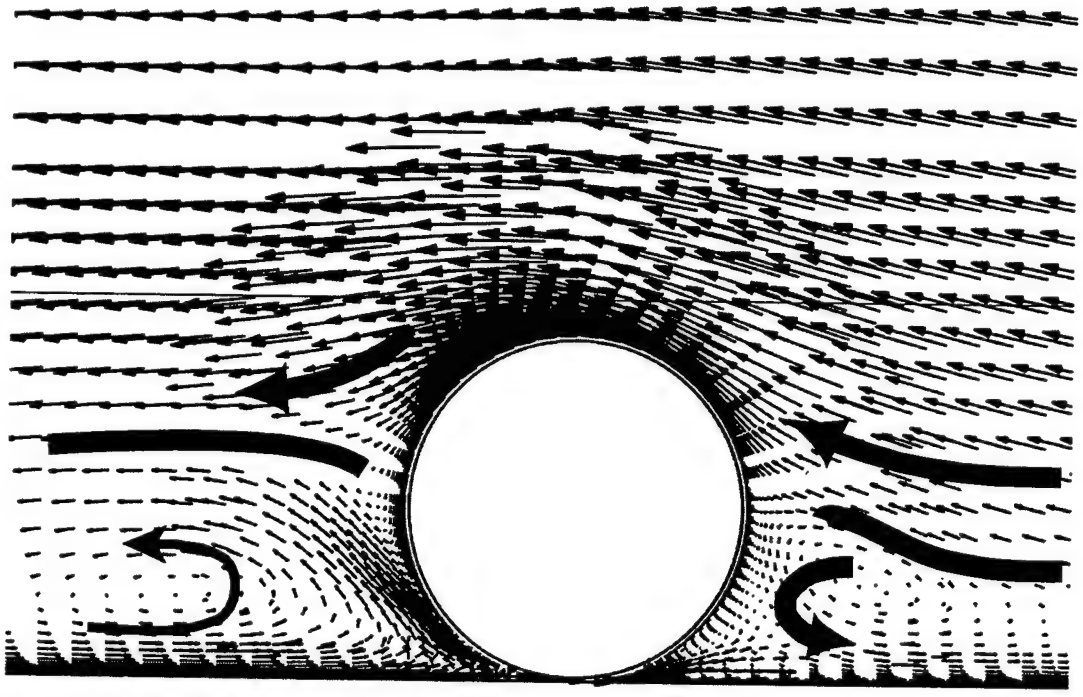

FIG. 36. Computed flow pattern for R = 27,000 and n = 0.6.

cylinder was evident (e.g. Fig. 25a). The flow is the result of the motion of the cylinder and wall surfaces drawing fluid away from the region near the contact point between the cylinder and wall. Continuity required flow to be directed into the region to compensate for the losses.

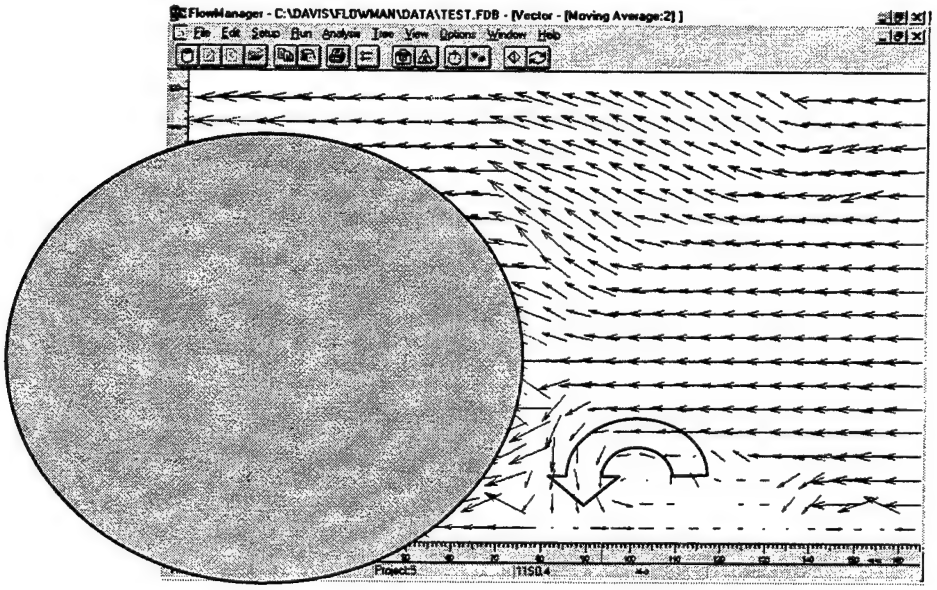

FIG. 37. Vortex measured on upstream side of the experiment cylinder similar to the simulation result. In the experiment, R = 42,000 and n = 0.60.

On the downstream side of the cylinder, for the case n = 0.60, and R = 27,000, a similar stagnation streamline exists (Fig. 36). It separates the flow coming over the crest of the cylinder from the flow forced up from the bed. Over the crest of the cylinder, the flow has not separated from the cylinder. The fluid streaming up from the bed appears to be the result of fluid drawn into the region near the contact point by the motion of the

cylinder and the bed. Continuity for incompressible fluids requires a flow outward from the region to compensate. Only a few of the PIV measurements showed this phenomena well. An example is given in Fig. 38. In almost all of the experiments, the flow over the crest of the cylinder plunged nearly to the bed.

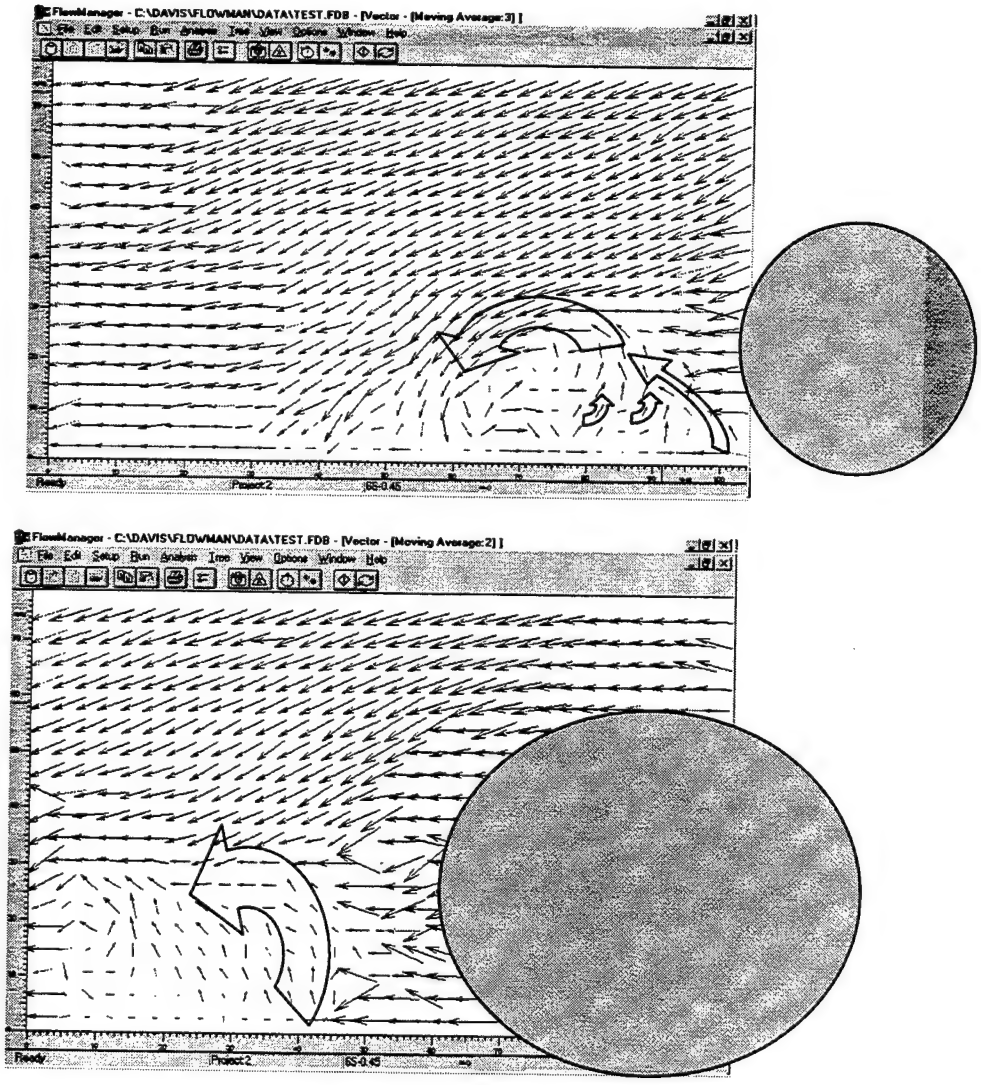

FIG. 38. Experimental measurements showing the streaming flow of water downstream of a rolling cylinder consistent with the numerical results.

To account for the discrepancy in the downstream flow patterns between the experimental and numerical results, the following reasoning is put forth, though it can not be verified by the available data in this study. The argument is that while separation is eliminated over the crest of the rolling cylinder, there is nothing to prevent the separation around the ends of the cylinder. Because of this separation, the pressure near the ends of the cylinder is lower than near the center of the cylinder and fluid moves from the center toward the ends.

It is conjectured here that the flow over the experiment cylinders plunges toward the bed on the downstream side of the cylinder where it then moves toward the ends of the cylinder. Hence, the wake away from the bed appears two dimensional (as discussed in Chapter III), but near the bed a stronger component of spanwise flow may be present. In the two-dimensional numerical simulation, this spanwise flow was not possible because two-dimensionality was imposed. Therefore, the fluid is forced out in front of (downstream of) the cylinder.

At least one experimental measurement suggested the presence of separation at the ends of the cylinders as shown in Fig. 39. In this image, the plane of the laser is close to the end of the cylinder. The vortical flow of the separation region around the ends of the cylinder would cause fluid to move upstream toward the cylinder in the separation zone as may be seen in the PIV measurement. A schematic drawing of the separation

zone at the end of the cylinder is provided in the inset figure of Fig. 39.

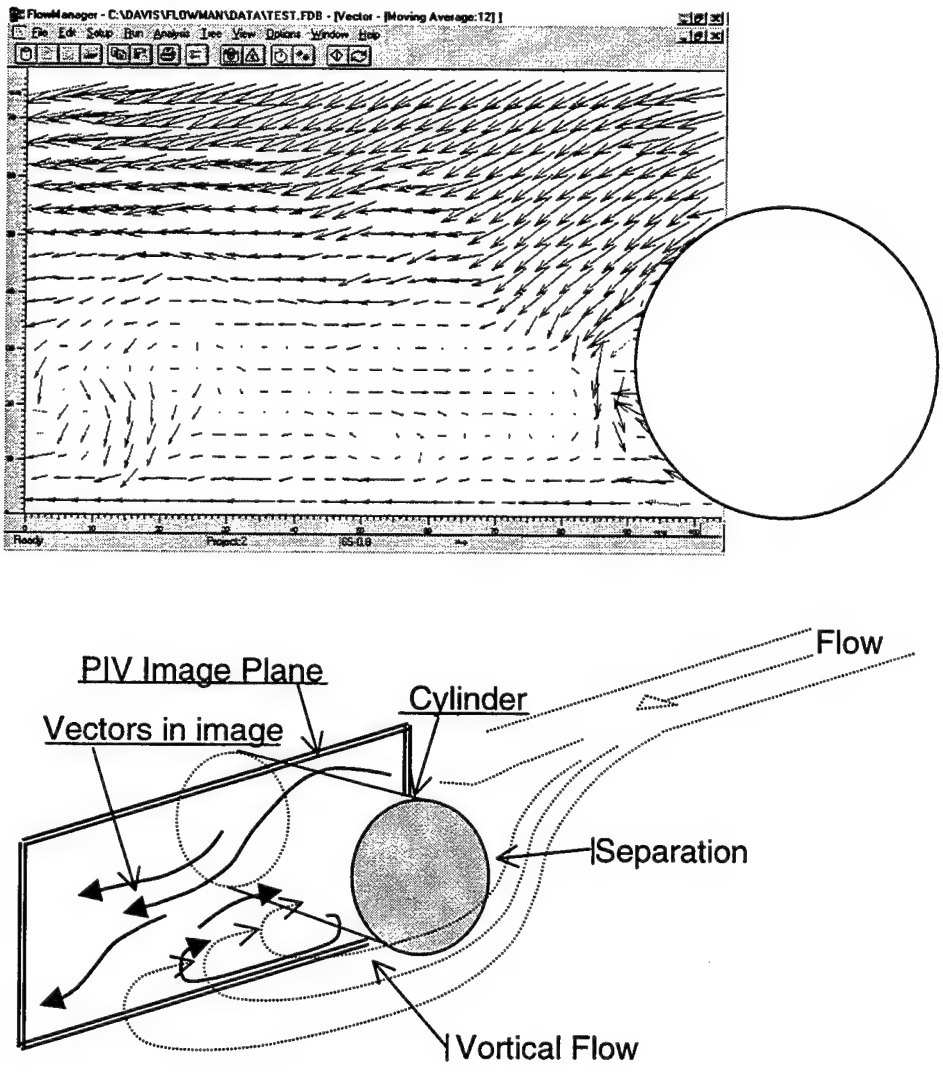

FIG. 39. Possible evidence of separated flow around the ends of the cylinder measured with the PIV.

As the value of n was increased to 0.71 and 0.8, the flow patterns changed slightly as can be seen when Fig. 36 is compared respectively to Figs. 40 and 41. The upstream

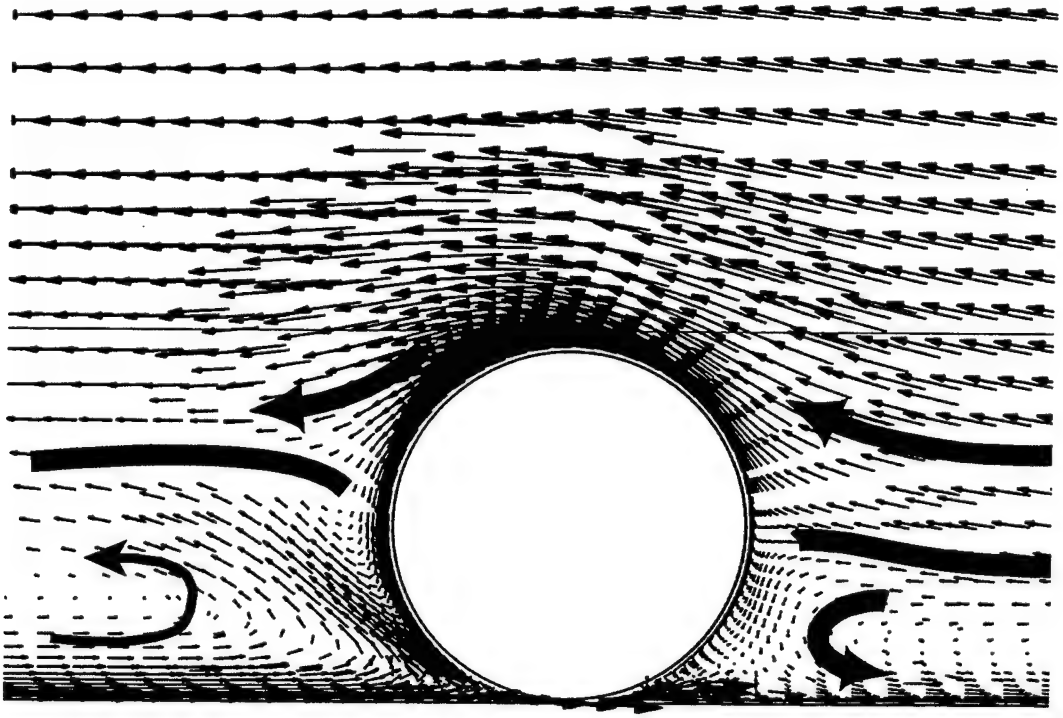

FIG. 40. Numerical results for R = 27000 and n = 0.71.

flow toward the cylinder (upstream) remained horizontal until nearer the cylinder as n was increased. The stagnation streamline on the upstream side of the cylinder was swept higher into the flow as n increased in order to capture more flow to replace the fluid being pulled out of the region near the contact point between the cylinder and the wall. Note that as n increased the flux of fluid from the contact region increased and the speed of the flow approaching the cylinder decreased. Therefore, more flow area had to be captured to replace the fluid moved out of the contact region. The flow patterns upstream of the cylinder for n = 0.71 and 0.80 were also similar to the flow patterns

observed in the PIV experiments.

On the downstream side of the cylinder for the higher values of n, the stream of fluid out from the contact point was pushed toward the bed. For the $n = 0.80$ condition, a small vortex was created immediately downstream of the cylinder near the bed.

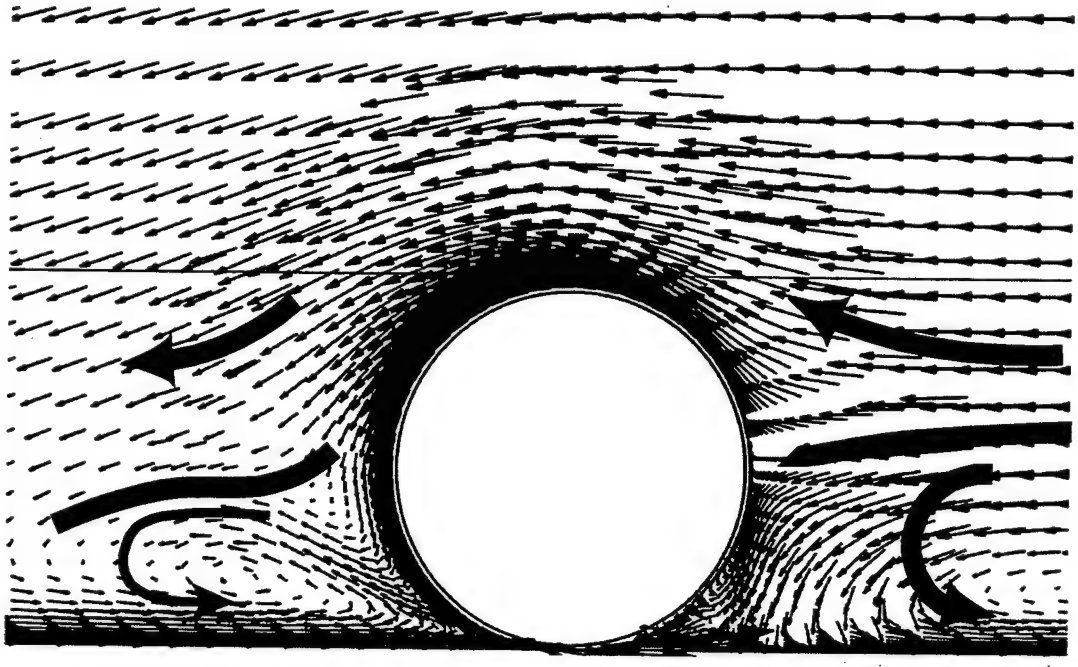

FIG. 41. Numerical results for $R = 27000$ and $n = 0.80$.

CHAPTER VI

SUMMARY & CONCLUSIONS

Summary

Motivated by a practical need to understand the motion of unexploded ordnance in aquatic environments, this research project was developed. Field investigations of unexploded ordnance suggested that ordnance (roughly shaped like finite-length cylinders) readily move about under the influence of hydrodynamic forces. The recommendations from the investigations suggested that a better understanding of the motion of ordnance might help to prioritize regional ordnance-removal efforts or to develop ordnance traps. A preliminary investigation of the literature on similar or related subjects produced virtually no directly applicable information.

Recognizing the void of information on the subject, this project was designed to develop a foundation upon which could be built future research on this subject. The problem was simplified to symmetrical, smooth, finite length cylinders in steady, uniform flows over a range of Reynolds numbers in a smooth-bottomed, horizontal flume. The properties measured, observed, or computed included the threshold velocity for incipient motion of the cylinders, the acceleration of the cylinders, the terminal velocity of the cylinders in given flows, the characteristics of the flow field around the cylinders, and the forces acting on the cylinders when rolling at terminal velocities. Future research can be expanded beyond and compared to this basic set of data. These results, though,

provide in themselves a basis for understanding and predicting cylinder behavior which will be useful for future investigations.

The research was divided into three areas which helped develop a circumspect understanding of the problem. One area was experimentation. Cylinders were released in a flume while the flow and the speed of the cylinder were measured. Two measurement techniques were used. The first used an acoustic Doppler velocimeter (ADV) to measure flows and a video camera to record the motion of the cylinders in the flume. The video images were processed to determine the speed and acceleration of the cylinders. The acceleration of the cylinder from rest would have provided valuable insight into the initiation of motion of a cylinder in other types of flow. However, the technique used to release the cylinders was not sufficient to provide a consistent starting condition and the image sampling rate that was used introduced artificial oscillations into the results. Therefore, cylinder acceleration data was not discussed. It was noted, however, that in all of the cases analyzed, the cylinders reached terminal velocity in about one second after release.

The terminal velocities of the cylinders were measured. Similar to sediment particles, a flow threshold had to be exceeded to initiate motion. The threshold was related to specific gravity and weakly related to cylinder diameter. At low values of the modified Shields parameter, θ_o, cylinders of like diameter with larger specific gravity

rolled more slowly than those with smaller specific gravity, and cylinders of same specific gravity but with larger diameters rolled more slowly than those with small diameter. However, at high values of θ_o, larger diameter cylinders rolled faster than smaller diameter cylinders due at least in part to the fact that the larger cylinders extend further outside the boundary layer where velocities are higher. At high θ_o, the terminal velocities of the cylinders were independent of θ_o, and were between 60-80% of the free-stream velocity. At lower θ_o, the speed of the cylinder depended on diameter, specific gravity and the free-stream velocity.

The video measurements did not provide information about the flow field around the cylinders, therefore additional measurements were made with a particle-image velocimetry (PIV) to record the flow field around the cylinders. The PIV measurements provided a view of the velocity field upstream and downstream of the rolling cylinders and some of the tests provided a measure of the cylinder speed which supported the video results. The PIV results showed that the flow does not separate from the surface of the rolling cylinder. The exact speed at which separation is completely suppressed was not determined, but the numerical results showed that even at terminal velocity ratio $n = 0.6$, the flow was not separating from the cylinder. The results verified expectations that separation would be suppressed based on the early work reported by Prandtl and Tietjens (1957) and Goldstein (1965), and the more recent work reported by Modi et al. (1990, 1991a, 1991b) and Munshi et al. (1996).

The second major area of research was the application of inviscid-flow theory to the problem. Once it was recognized that the flow did not separate from the crest of the cylinders and that the boundary layer was confined to a thin region very near the cylinder and that the downstream wake was reasonably two-dimensional, the application of an inviscid-flow formulation to the problem seemed justifiable. Investigation of previous research yielded the Milne-Thomson (1968) formulation for an infinitely long cylinder resting on a wall. The formula was applied to find the speed at which a cylinder must roll so that everywhere the cylinder's surface is moving as fast or faster than the fluid adjacent to it. Under these conditions, it was assumed that separation would be suppressed, therefore the drag would be minimal, and the cylinder would have reached a maximum value for terminal velocity. In this way, it was found that the terminal velocity of a cylinder should be about 71% of the free-stream velocity. This compared well with the results of the experimental data that showed terminal velocities are between 60-80% of the free-stream velocity.

The third major area of research, was an investigation of the fluid forces acting on the cylinders at or near their terminal velocities. This was accomplished through numerical simulation using a model developed around the Reynolds-Averaged Navier-Stokes equations. The simulations considered an infinitely-long cylinder (assumes two-dimensional wake) in a steady, uniform flow. The simulations showed that at the terminal velocity of 71% of the free stream flow, the pressure and shear forces acting on

the cylinders were of similar magnitude and small. The moment on the cylinder about the contact point between the cylinder and the bed was nearly zero. The results further indicated that cylinders rolling at slower speeds (e.g., 60% of the free stream velocity) had accelerating forces and moments acting on them while cylinders rolling at higher speeds (e.g., 80% of the free-stream velocity) had decelerating forces and moments acting on them. These results were in-line with experimental observations. The simulations showed that at low Reynolds numbers (R) the cylinders should roll at speeds near 70% of the free-stream flow which was also verified by the experiments.

Conclusions

Given the results of the research outlined above the following conclusions can be made about the characteristics of the motion of unrestrained cylinders in flows. Even though the circular cylinders were smooth and rolled over a smooth bed, a critical threshold free-stream velocity was required to induce the cylinders to roll. The critical velocity was strongly related to the specific gravity of the cylinders and to a lesser extent the diameter of the cylinder. The results are consistent with observations of spherical particles in flows, where heavier particles have a higher critical threshold (van Rijn 1984). The critical threshold in a natural setting with a rough bed (sand, clay, etc.), rough cylinder surfaces (e.g., ordnance covered in marine growth or corroded), and unsteady flow conditions would be much higher due to the increased resistence. Prior research (Brown 1967 and Font 1967) provides drag coefficients between 0.55 and 0.93 for

cylinders on a wall which could be used to estimate the force on a cylinder on a bed if fully exposed to the flow. The coefficients should be decreased to account for the small aspect ratio of the cylinders consistent with the influence of aspect ratio on drag coefficients reported by Goldstein (1965).

Based on literature reviews and qualitative observations of the motion of the cylinders, the greatest drag and lift forces occur on the cylinders when they are at rest on the wall in the flow. Once the cylinder begins to move the drag force will decrease because the relative flow velocity around the cylinder decreases and because the movement of the cylinder's surface will reduce the size of the wake downstream by delaying separation. Regarding lift, while rotation can induce lift on a cylinder in a flow, it is secondary to the lift induced by the free-stream flow around the cylinder in the presence of the wall. Previous studies by van Rijn (1984) using spheres suggested that the influence of rotation on lift was an order of magnitude lower than the influence of the free-stream velocity. The experimental observations in this study, showed that under high free-stream velocities, the cylinders would lift off the bed while attempts were made to hold them in place prior to release. Once released, however, the cylinders did not lift off the bed suggesting that the increase in lift due to increased rotation of the cylinder was not sufficient to offset the reduction in lift due to the decreased relative flow past the cylinder.

The ratio n of the cylinder velocity to the free-stream velocity asymptotically approached a constant value at high values of R or θ_o. The data values for maximum n were between 0.6 and 0.8, and the inviscid-flow derivations and numerical results each suggested a maximum velocity close to $n = 0.7$. At lower values of θ_o, n is below 0.7. Additionally, it was observed that cylinders accelerated rapidly to their terminal velocities. In most cases, they achieved terminal velocity in about one second. This suggests that cylinders will adjust quickly to changes in flow conditions. For example, under long-period, shallow-water waves where the bed velocity is directed forward and backward for several seconds, cylinders would have ample time to achieve a terminal velocity. Further, considering the results of the experiments, if a high value of θ_o existed say under the crest of the wave, the cylinder might ideally reach a speed of 70% of the flow velocity. However under the trough where the θ_o might be lower, the cylinder might reach velocities that are lower, say 40% of the flow velocity. Therefore, depending on the particular flow conditions, cylinders may travel further in one direction than the other. Note though that this speculative argument does not consider other phenomena, such as decelerating the cylinder to reverse its direction or the influence of incipient motion thresholds for different bed or cylinder roughnesses.

Finally, in most of the PIV measurements, the fluid over the crest of the cylinder looked two-dimensional and similar to the result expected from inviscid-flow theory (i.e., tangential to the cylinder surface) and impinged on the bed of the flume. In fact, the

control area calculations that were made suggested the flow was indeed two-dimensional. The PIV-measured flow patterns, however, were in contrast with the numerical results that suggested a two-dimensional flow downstream of a cylinder will require the slower moving fluid near the bed (boundary layer fluid) to be pushed out in front of the cylinder as it rolls. Therefore, while not proven, it was conjectured that in the experiments, the fluid in the wake of the cylinder may have been largely two-dimensional away from the bed, but where it impinged on the bed, it was in part driven toward the ends of the cylinder by the lower pressure that must exist there because of separation around the ends of the short aspect ratio cylinders. Hence, the flow downstream of the cylinders in the experiments may have been more complex than was actually captured by the PIV measurements. Future experiments should explore this phenomena.

Ultimately, future investigators will want to consider the motion of asymmetrical cylinders on roughened beds and unsteady flows (namely periodic flows) to more directly address the issue of transport of unexploded ordnance in aquatic environments. However, prior to those investigations additional simplified experiments should be conducted. First, techniques should be developed to measure the forces on the cylinders in laboratory experiments. This might be done by developing experiments similar to the numerical simulation approach used in this study where the cylinder (instrumented for force measurements) is held in place while it is rotated over a moving bed. For given flows, the rotation that yields reasonably small moments and forces could be determined while

the flow field around the cylinder is recorded. The value of n at which separation is initially suppressed could also be determined. Second, additional simulations could be conducted to extend the results of this study (i.e., increased ranges of R and n). A short aspect-ratio cylinder could be modeled in a three-dimensional simulation, and the acceleration of the cylinder to terminal velocity could be simulated. With these successful simulations completed, the acceleration, terminal velocity, and variation of forces acting on an asymmetrical ordnance piece (cylinder with pointed end) could be conducted to determine the influence of the asymmetry on ordnance behavior. Finally, laboratory studies of cylinders or ordnance on rough surfaces and in unsteady, non-uniform flows could be conducted, followed by field experiments. While the research documented in this report is enlightening and has clarified some of the phenomena associated with the unrestrained motion of cylinders in flows, much more research is required to fully understand the movement of ordnance or other cylindrical objects in natural aquatic environments.

REFERENCES

Arie, M., and Kiya, M. (1967). "Lift of a cylinder in shear flow subject to an interference of a plane wall." *Trans. of the Japan Soc. of Mech. Eng.*, 33(246), 242-248.

Badr, H. M., Coutanceau, M., Dennis, S. C. R., and Menard, C. (1990). "Unsteady flow past a rotating circular cylinder at Reynolds numbers 10^3 and 10^4." *J. of Fluid Mech.*, 220, 459-484.

Bearman, P. W., and Zdravkovich, M. M. (1978). "Flow around a circular cylinder near a plane boundary." *J. of Fluid Mech.*, 89(1), 33-47.

Brown, J. (1967). "Hydrodynamic forces on a submarine pipeline." *J. of the Pipeline Div.*, ASCE, 93(PL1), 9-19.

Chen, H. C., Patel, V. C., and Ju, S. (1990). "Solutions of Reynolds-averaged Navier-Stokes equations for three-dimensional incompressible flows." *J. of Computational Physics*, 88(2), 305-336.

Cornish, J. J. III, and Jex, H. (1968). "Some aerodynamic characteristics of land vehicles." *Proc. of AIAA Symp. on Aerodynamics of Sports and Competition Automobiles,* Los Angeles, CA, 81-86.

Davis, D. A., and Ciani, J. B. (1976). "Wave forces on submerged pipelines - A review with design aids." *Tech. Report R844*, U.S. Navy Naval Facilities Engineering Command, Civil Engineering Laboratory, Port Hueneme, CA.

Fahnestock, R. K., and Haushild, W. L. (1962). "Flume studies of the transport of pebbles and cobbles on a sand bed." *Geol. Soc. of America Bulletin*, 73, November, 1431-1436.

Fenical, S. A. (1996). "Experimental studies of unrestrained cylinders on an impermeable bottom under currents." *M.S. thesis,* Texas A&M University, College Station, TX.

Font, J. B. (1967). "Discussion of 'Hydrodynamic forces on a submarine pipeline,' by R. J. Brown." *J. of the Pipeline Division*, ASCE, 93(PL3), 77-79.

Fredsøe, J., and Hansen, E. A. (1987). "Lift forces on pipelines in steady flow." *J. of Waterway, Port, Coastal and Ocean Eng.*, 113(2), 139-155.

Goldstein, S., Ed. (1965). *Modern Developments in Fluid Dynamics: An Account of Theory and Experiment Relating to Boundary Layers, Turbulent Motion, and Wakes.* Dover Publications, Inc., New York, NY.

Grace, R. A. (1971). "The effects of clearance and orientation on wave-induced forces on pipelines: Results of laboratory experiments." *Tech. Report No. 15 U Hawaii-Look-Lab-71-15*, University of Hawaii, Honolulu, HI.

Hafen, B. (1975). "Forces on a transverse circular cylinder in a steady uniform flow near a plane boundary." *M.S. thesis*, Oregon State University, Corvallis, OR.

Havelock, T.H. (1949). "The resistance of a submerged cylinder in accelerated motion." *The Collected Papers of Sir Thomas Havelock on Hydrodynamics*, Office of Naval Research, Department of the Navy, ONR/ACR-103, Arlington, VA.

Hubbard, B. J. (1994). "A chimera RANS methodology for steady and unsteady incompressible viscous flows." *PhD dissertation,* Texas A&M University, College Station, TX.

Knoll, D., and Herbich, J. (1980). "Wave and current forces on a submerged offshore pipeline." *Offshore Technology Conf.*, OTC 3762, 227-331, Houston, TX.

Lee, H-Y. and Hsu, I-S. (1994). "Investigation of saltating particle motions." *J. of Hydraulic Eng., ASCE*, 120(7), 831-845.

Milne-Thomson, L. M. (1968). *Theoretical Hydrodynamics.* The MacMillan Co., Inc., New York, NY.

Modi, V. J., Mokhtarian, F., and Yokomizo, T. (1990). "Effect of moving surfaces on the airfoil boundary-layer control." *J. of Aircraft*, 27(1), 42-50.

Modi, V. J., Fernando, M. S. U. K., and Yokomizo, T. (1991a). "Moving surface boundary-layer control: Studies with bluff bodies and application." *AIAA Journal*, 29(9), 1400-1406.

Modi, V. J., Mokhtarian, F., Fernando, M. S. U. K., and Yokomizo, T. (1991b). "Moving surface boundary-layer control as applied to two-dimensional airfoils." *J. of Aircraft*, 28(2), 104-112.

Munshi, S. R., Modi, V. J., and Yokomizo, T. (1996). "Effect of momentum injection

on the drag reduction and flow-induced instabilities of a square prism." *Int. J. of Offshore and Polar Eng.*, 6(3), 161-170.

Okamoto, S., and Sunabashiri, Y. (1992). "Vortex shedding from a circular cylinder of finite length placed on a ground plane." *Trans. of the American Soc. of Mech. Eng.*, 114, 512-521.

Pope, J., Lewis, R. D., and Welp, T. (1996). "Beach and underwater occurrences of ordnance at a former defense site: Erie Army Depot, Ohio." *Tech. Report CERC-96-1,* US Army Engineer Waterways Experiment Station, Vicksburg, MS.

Prandtl, L., and Tietjens, O. G. (1957). *Applied Hydro- and Aeromechanics.* Dover Publications, Inc., New York, NY.

Rasband, W. (1994). *NIH Image 1.52 Software Manual.* NIH Publishing, Chicago, IL.

Riedl, S. J. (1994). "Application of optical remote sensing to the measurement of wave surface kinematics." *M.S. thesis*, Texas A&M University, College Station, TX.

Rooney, D. M., Rodichok, J., and Dolan, K. (1995). "Finite aspect ratio effects on vortex shedding behind two cylinders at angles of incidence." *J. of Fluids Eng.,* Trans. of the ASME, 117, June, 219-226.

Saffman, P. G. (1965). "The lift on a small sphere in a slow shear flow." *J. of Fluid Mech.*, 22(2), 385-400.

Sarpkaya, T., and Isaacson, M. (1981). *Mechanics of Wave Forces on Offshore Structures.* Von Nostrand Reinhold Company, Inc., New York, NY.

Sarpkaya, T., and Rajabi, F. (1979). "Hydrodynamic drag on bottom-mounted smooth and rough cylinders in periodic flow." *Offshore Tech. Conf.*, OTC 3761, 219-226, Houston, TX.

Schlichting, H. (1968). *Boundary Layer Theory.* McGraw-Hill Book Co., Inc., New York, NY.

Shields, A. (1936). "Application of the theory of similarity and turbulence research to the bed load movement." *Mitt. Preuss. Vers. Wasser Schiff.*, 26.

Skotner, C., Jonsson, I. G., and Skourup, J. (1994). "Wave forces on a large, horizontal submerged cylinder." *Ocean Engineering*, 21, p 711.

Suhs, N. E., and Tramel, R. W. (1991). "PEGSUS 4.0 User's Manual." *Tech. Report AEDC-TR-91-8*, Arnold Engineering Development Center, Arnold Airforce Base, TN.

Sumer, B. M., Jensen, B. L., and Fredsøe, J. (1991). "Effect of a plane boundary on oscillatory flow around a circular cylinder." *J. of Fluid Mech.*, 225, 271-300.

Taniguchi, S., and Miyakoshi, K. (1990). "Fluctuating fluid forces acting on a circular cylinder and interference with a plane wall." *Experiments in Fluids*, 9, 197-204.

Tezduyar, T. E., Behr, M., and Liou, J. (1992a). "A new strategy for finite element computations involving moving boundaries and interfaces - the deforming-spatial-domain / space-time procedure: I. The concept and the preliminary numerical tests." *Computer Methods in Applied Mechanics and Engineering*, 92, 339-351.

Tezduyar, T. E., Behr, M., Mittal, S., and Liou, J. (1992b). "A new strategy for finite element computations involving moving boundaries and interfaces - the deforming-spatial-domain / space-time procedure: II. Computation of free-surface flows, two-liquid flows, and flows with drifting cylinders." *Computer Methods in Applied Mechanics and Engineering,* 92, 353-371.

Thwaites, B. (1960). *Incompressible Aerodynamics*. Oxford University Press, Oxford, Great Britain.

Tokumaru, P. T., and Dimotakis, P. E. (1993). "The lift of a cylinder executing rotary motions in a uniform flow." *J. of Fluid Mech.*, 255, 1-10.

van Rijn, L. (1984). "Sediment transport, Part I: Bed load transport." *J. of Hydraulic Eng.*, ASCE, 110(10), 1431-1456.

Vinokur, M. (1980). "On one-dimensional stretching functions for finite-difference calculations." *NASA Contract Report 3313*, NASA Ames Research Center, Moffett Field, CA.

Wright, J. C., and Yamamoto, T. (1979). "Wave forces on cylinders near plane boundaries." *J. of Waterway, Port, Coastal and Ocean Eng.*, ASCE, 105(WW1), 1-13.

Yamamoto, T., and Nath, J. H. (1973). "Fluid dynamic flow around pipelines." *Report 46*, Engineering Experiment Station, Oregon State University, Corvallis, OR.

Yamamoto, T., Nath, J. H., and Slotta, L. S. (1973). "Yet another report on cylinder drag or wave forces on horizontal submerged cylinders." *Bulletin No. 47,* Engineering Experiment Station, Oregon State University, Corvallis, OR.

Yamamoto, T., Nath, J. H., and Slotta, L. S. (1974). "Wave forces on cylinders near plane boundary." *J. of the Waterways, Harbors and Coastal Eng. Div.,* ASCE, 100(WW4), 345-359.

APPENDIX I

NOTATION

The following symbols are used in this report:

a = cylinder radius

g = acceleration due to gravity

C_D = drag force coefficient

$C_{D\infty}$= drag force coefficient for infinitely long cylinder

C_L = lift force coefficient

C_x = x-directed force due to pressure and shear

C_{xp} = x-directed force due to pressure

$C_{x\tau}$ = x-directed force due to shear

C_y = y-directed force due to pressure and shear

C_{yp} = y-directed force due to pressure

$C_{y\tau}$ = y-directed force due to shear

C_m = moment about the contact point due to pressure and shear

C_{mp}= moment about the contact point due to pressure

$C_{m\tau}$= moment about the contact point due to shear

C_μ = numerical simulation constant

D = diameter of cylinder

e = net flow error in control areas

F_D = drag force

F_L = lift force

i = complex number

k = turbulence kinetic energy

L = length of cylinder

L^* = characteristic length scale

n = ratio of cylinder velocity to free-stream velocity

P = mean pressure

p = turbulent fluctuation about mean pressure

$\tilde{p}$ = instantaneous pressure

q = potential flow velocity

q_o = flux out of control area

q_i = flux into control area

R = Reynolds number

r = radial distance

S = specific gravity of cylinders

U = flow velocity or mean flow velocity

U_c = critical threshold velocity for incipient motion of cylinder

U^j = j^{th} mean velocity component

U_i^j = j^{th} mean velocity component differentiated with respect to the i^{th} direction component

U_o^j = j^{th} mean velocity component differentiated with respect to time

U_o = free-stream velocity

U_r = relative velocity between cylinder and free stream

U^* = characteristic velocity scale

u = x-directed velocity or turbulent fluctuation about mean velocity

$\tilde{u}^i$ = ith direction component of instantaneous velocity

$\tilde{u}^i_j$ = ith direction component of instantaneous velocity differentiated with respect to jth direction

$\tilde{u}^i_o$ = ith direction component of instantaneous velocity differentiated with respect to time

u_* = friction velocity

V = linear velocity of cylinder

V_i = linear velocity of cylinder at ith time step

v = y-directed velocity

w = complex potential function

$\overline{w}$ = conjugate of the complex potential function w

X_i = linear position of cylinder for time step i

X_{ij} = linear position for time step i of marker j on end of cylinder

x = abscissa, coordinate position

y = ordinate, coordinate position, distance from wall

y^+ = non-dimensional cell height

z = complex number, $x + iy$

$\overline{z}$ = conjugate of the complex number z

Δt = time step (inverse of the sampling rate)

Δx = distance increment in the x direction

Δy = distance increment in the y direction

δ_{ij} = kroenecker delta function

ε = turbulence kinetic energy dissipation rate

θ_c = Shields parameter based on critical threshold velocity

θ_i = angular position of cylinder for time step i

θ_{ij} = angular position for time step i of marker j on end of cylinder

θ_o = Shields parameter based on free-stream velocity

ν_t = eddy viscosity due to turbulence

ν = fluid kinematic viscosity

ρ = density of water

ω = angular velocity of cylinder

ω_i = angular velocity of cylinder at time step i

ω_{ij} = angular velocity for time step i of marker j on end of cylinder

APPENDIX II

COPYRIGHT PERMISSION

Fax Transmittal Sheet
of the

Waterways Experiment Station
Coastal & Hydraulics Laboratory
Coastal Sediments & Engineering Division

3909 Halls Ferry Rd
Vicksburg MS 39180-6199
e-mail: j.davis@cerc.wes.army.mil

18 October 1999

TO	**FROM**
Name: **Karen Ryan, ASCE**	Name: **Jack E. Davis (CEERD-HC-S)**
Tel: (703) 295-6300	Tel: 601/634-3006
Fax: (703) 295-6278	Fax: 601/634-3080

Number of Pages : 1

COMMENTS
Dear Ms. Ryan,

I am a doctoral candidate at Texas A&M University and I will be finalizing my dissertation in the next few weeks. Our library sends our dissertation to University Microfilms Inc., for preparation of a microfilm copy of the document. As I am sure you are aware, UMI retains the right to sell both hard and microfilm copies of the document.

My reason for writing is to request permission to use information from the manuscript I published in your journal (co-authored with Scott Fenical, Jun Zhang, and Billy Edge). The article appeared in the September 1999 Issue of the Journal of Hydraulic Engineering (Vol. 125, No. 9) on pages 943-952. Much of the information in the journal articles appears in the first three chapters of my dissertation.

Thank you very much for your assistance,

Jack E. Davis
Member, No. 265351

ASCE
American Society of Civil Engineers

October 20, 1999

Mr. Jack E. Davis
Waterways Experiment Station
Coastal and Hydraulics Laboratory
3909 Halls Ferry Road
Vicksburg, MS 39180-6199

Dear Mr. Davis:

Permission is granted for the use of the ASCE copyrighted material as requested in your letter (copy attached). This one time grant is subject to the following conditions:

(1) A credit line, which must be added to the material being reprinted must include title, author, book/journal name, publication date and must indicate that the material is reproduced by permission of the publisher (ASCE).
(2) The fee is waived.

If you decide not to use this material, please advise the grantor (ASCE) within 30 days.

Sincerely,

Karen A. Ryan
Copyrights and Permissions
American Society of Civil Engineers
1801 Alexander Bell Drive
Reston, VA 20191
(703) 295-6212
Fax (703) 295-6278
kryan@asce.org

1999
Civil Engineering Convention & Exposition
Leading the Race in Management, Practice & Technology

VITA

Jack Edward Davis
125 Timberwood Dr.
Raymond, MS 39154-8002

Education:
B.S., Civil Engineering, University of Illinois at Urbana-Champaign, 1983
M.S., Civil Engineering, The University of Texas at Austin, 1990
PhD, Ocean Engineering, Texas A&M University, 1999

Experience 1984-1999:
U.S. Army Waterways Experiment Station, Coastal & Hydraulics Laboratory. Work has included physical modeling of river structures, numerical modeling of reservoir water quality, numerical wind-wave generation and transformation, coastal structures evaluation and design, wetland hydrology, wetland restoration, and dredging and dredged -material uses.

Selected Publications:
Davis, J. E., Fenical, S. A., Zhang, J., and Edge, B. L. (1999). "Terminal velocity of unrestrained cylinders in flows." *J. of Hydraulics*, ASCE, 125(9), 943-952.

Davis, J. E. (1997). "Checklist for planning wetland erosion control." *Proc. of the Wetlands Engineering and River Restoration Conf.*, ASCE, Denver, CO.

Davis, J. E., and Landin, M. C. (1996). "Proceedings of the National Workshop on Geotextile Tube Applications." Tech. Report, WRP-RE-17, U.S. Army Engineer Waterways Experiment Station, Vicksburg, MS.

Davis, J. E., and Landin, M. C. (1998). "Geotextile tube structures for wetlands restoration and protection." *Proc. of the 17th WEDA Conf.*, New Orleans, LA, 429-437.

Davis, J. E., (1990). "The design and modeling of side weirs for detention basin facilities." *M.S. thesis*, Univ. of Texas, Austin, TX.

Davis, J. E., Smith, J. M., and Vincent, C. L., (1991). "Parametric description for a wave energy spectrum in the surf zone." Misc. Paper, CERC-91-11,U.S. Army Engineer Waterways Experiment Station, Vicksburg, MS.

REPORT DOCUMENTATION PAGE

Form Approved
OMB No. 0704-0188

1. REPORT DATE *(DD-MM-YYYY)*	2. REPORT TYPE	3. DATES COVERED *(From - To)*
April 2000	Final report	

4. TITLE AND SUBTITLE
Unrestrained Cylinders Rolling in Steady Uniform Flows

5a. CONTRACT NUMBER

5b. GRANT NUMBER

5c. PROGRAM ELEMENT NUMBER

6. AUTHOR(S)
Jack E. Davis

5d. PROJECT NUMBER

5e. TASK NUMBER

5f. WORK UNIT NUMBER

7. PERFORMING ORGANIZATION NAME(S) AND ADDRESS(ES)

U.S. Army Engineer Research and Development Center
Coastal and Hydraulics Laboratory
3909 Halls Ferry Road
Vicksburg, MS 39180-6199

8. PERFORMING ORGANIZATION REPORT NUMBER

ERDC/CHL TR-00-7

9. SPONSORING / MONITORING AGENCY NAME(S) AND ADDRESS(ES)
U.S. Army Corps of Engineers
Washington, DC 20314-1000

10. SPONSOR/MONITOR'S ACRONYM(S)

11. SPONSOR/MONITOR'S REPORT NUMBER(S)

12. DISTRIBUTION / AVAILABILITY STATEMENT

Approved for public release, distribution unlimited.

13. SUPPLEMENTARY NOTES

14. ABSTRACT

Ordnance remediation projects for underwater sites have suggested that understanding the motion of cylinders (the approximate shape of ordnance) in flows would help to predict regions of ordnance mobility, prioritize remediation efforts, and improve the design of engineering works trap ordnance. Therefore, to develop a better understanding of the motion of cylinders, the characteristics of motion of smooth, unrestrained cylinders in contact with a smooth horizontal bed were investigated in a flume with steady, uniform flows. Inviscid-flow theory was used to estimate maximum cylinder velocities and numerical simulations were used to understand the hydrodynamic forces on the cylinders. Eight cylinders were used in the laboratory experiments having varying specific gravities and diameters.

At low velocities, experiments showed that the cylinders follow trends similar to those noted in sediment particle studies. Incipient motion velocities were highest for the heavier cylinders. At high flows, the terminal velocity of the cylinders was limited to between 60-80 percent of the free stream flow. The cylinders accelerated to their maximum velocities within about one second. Inviscid-flow theory derivations implied that the maximum velocity of the cylinder would be 71 percent of the free stream flow which was consistent with the experiments. Use of potential flow theory was assumed valid (as an estimator) because experiments verified that flow over the

(continued)

15. SUBJECT TERMS

16. SECURITY CLASSIFICATION OF:			17. LIMITATION OF ABSTRACT	18. NUMBER OF PAGES	19a. NAME OF RESPONSIBLE PERSON
a. REPORT	b. ABSTRACT	c. THIS PAGE			19b. TELEPHONE NUMBER *(include area code)*
UNCLASSIFIED	UNCLASSIFIED	UNCLASSIFIED		134	

rolling cylinder did not separate from the cylinder surface and that they were reasonably two-dimensional. The numerical results showed that separation from the cylinder would be eliminated by the moving surface of the cylinder. In fact, suppression of separation occurred even when the cylinder was rolling at only 60 percent of the free-stream flow velocity. The simulations were two-dimensional but showed that the moment about the contact point between the cylinder and the wall was nearly zero and that the downstream directed force on the cylinder was small under the terminal velocity conditions measured in the experiments.